JCI insight

ANGPTL8 has both endocrine and autocrine effects on substrate utilization

Federico Oldoni, … , Jonathan C. Cohen, Helen H. Hobbs

JCI Insight. 2020. https://doi.org/10.1172/jci.insight.138777.

Research In-Press Preview Endocrinology Metabolism

Graphical abstract

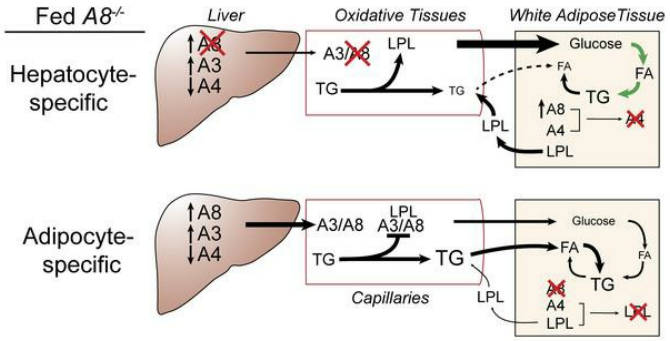

ANGPTL8 has Both Endocrine and Autocrine Effects on Substrate Utilization

Federico Oldoni[1*], Haili Cheng[1*], Serena Banfi[1], Viktoria Gusarova[2], Jonathan C. Cohen[3], and Helen H. Hobbs[1,4]

[*]These authors contributed equally to this work. [1]Departments of Molecular Genetics and Internal Medicine, [2]Regeneron Pharmaceuticals, Tarrytown, NY 10591, [3]The Center for Human Nutrition, and [4]Howard Hughes Medical Institute, University of Texas Southwestern Medical Center, Dallas, TX 75390

The authors have declared that no conflict of interest exists.

Abstract

The angiopoietin-like protein ANGPTL8 (A8) is one of three ANGPTLs (A8, A3, A4) that coordinate changes in triglyceride (TG) delivery to tissues by inhibiting lipoprotein lipase (LPL), an enzyme that hydrolyzes TG. Previously we showed that A8, which is expressed in liver and adipose tissue, is required to redirect dietary TG from oxidative to storage tissues following food intake. Here we show that A8 from liver and adipose tissue have different roles in this process. Mice lacking hepatic A8 have no circulating A8, high intravascular LPL activity, low plasma TG levels, and evidence of decreased delivery of dietary lipids to adipose tissue. In contrast, mice lacking A8 in adipose tissue have higher postprandial TG levels and no alteration in fatty acid composition in adipocytes. Expression of A8, together with A4, in cultured cells reduced A4 secretion and A4-mediated LPL inhibition. Thus, hepatic A8 (with A3) acts in an endocrine fashion to inhibit intravascular LPL in oxidative tissues, whereas A8 in adipose tissue enhances LPL activity by autocrine/paracrine inhibition of A4. These combined actions of A8 ensure that TG stores are rapidly replenished and sufficient energy is available until the next meal.

Introduction

Fatty acids from the diet or synthesized *de novo* are esterified with glycerol to form triglycerides (TG), the major energy reservoir in vertebrates. In enterocytes and hepatocytes, TGs are packaged with other lipids and proteins and secreted into the circulation as components of chylomicrons or VLDL (1, 2). Lipoprotein lipase (LPL), an enzyme residing on the endothelial surfaces of capillaries, hydrolyzes circulating TG, releasing fatty acids for uptake by adjacent tissues (3, 4). The fraction of TG-derived fatty acids delivered to each tissue is determined by LPL activity in that tissue (5). In fasted animals, fatty acids are delivered predominantly to oxidative tissues (muscle, heart, brown fat) where LPL activity is high (5, 6). In the fed state, LPL activity is suppressed in oxidative tissues so that more fatty acids traffic to white adipose tissue (WAT) (5, 6). Uptake of fatty acids into WAT is 10-fold higher in fed mice than in fasting animals (7).

The rapid changes in LPL activity in tissues in response to nutritional intake are mediated primarily at the post-translational level (8) by three members of the angiopoietin-like protein (ANGPTL) family of secreted proteins: ANGPTL3 (A3), ANGPTL4 (A4), and ANGPTL8 (A8) (9-11). All three proteins inhibit LPL *in vitro*, albeit with different potencies (12-14). The ANGPTLs are expressed in a tissue-specific manner and levels of expression depend on nutritional cues (7, 15, 16). All three proteins are highly expressed in liver. Whereas A3 expression is restricted almost exclusively to liver (9, 17), A4 and A8 are also expressed at high levels in adipose tissue (11, 15, 18-20). Feeding elicits dramatic and reciprocal changes in A4 and A8 mRNA levels. Levels of A4 mRNA increase in WAT during fasting and fall upon refeeding (15), whereas expression of A8 is barely detectable in the tissues of fasted animals, but increases rapidly upon refeeding (11, 19, 20). Levels of A3 mRNA in the liver are consistently higher than those of either A4 or A8, and change more modestly in response to food intake (21).

A4 and A3 have similar overall structures. Both contain a proprotein convertase site and can undergo catalytic cleavage, producing an N-terminal coiled-coil domain that contains an LPL interaction site, and a C-terminal fibrinogen-like domain (22). A8, unlike A3 or A4, does not contain a fibrinogen-like domain. A4 is a more potent inhibitor of LPL *in vitro* and *in vivo* than the other two family members (13, 14) and is essential for the fasting-induced suppression of intravascular lipolysis (15). A4 also stimulates intracellular lipolysis in WAT (23, 24). Thus, A4 expression in WAT promotes flux of fatty acids towards oxidative tissues to supply them with energy substrate during fasting.

A3 and A8 are functionally interdependent *in vivo* (11) and *in vitro* (25). Expression of A8 fails to suppress intravascular LPL of mice lacking A3 (11). The two family members form a complex in which the LPL binding domain of A8 (and not A3) is required for LPL inhibition (25). After feeding, A3 and A8 act together in the systemic circulation to inhibit LPL activity. Under these conditions, more circulating TGs bypass oxidative tissues and are hydrolyzed in WAT (7, 21). Feeding also increases expression of A8 in adipose tissue, but its role in WAT has not been defined (11, 19, 20).

To begin to understand the relative roles of A8 in liver and in adipose tissue, we developed mice in which A8 is selectively inactivated in those two tissues. Here we show that A8 has distinct physiological functions in the two tissues. All detectable circulating A8 originates in the liver and only this form of A8 complexes with A3 to inhibit intravascular lipolysis. A8 from adipose tissue makes no detectable contribution to circulating A8, but rather has local effects on substrate homeostasis. A8 expression in adipose tissue attenuates the LPL inhibitory actions of A4, thus ensuring a rapid replenishment of energy stores during the next fast.

Results

Tissue-specific inactivation of A8. We developed C57BL/6N mice in which expression of A8 was ablated either in hepatocytes [Liver-specific (Ls)-*A8*$^{-/-}$ mice] or in adipocytes [Adipose-specific (As)-*A8*$^{-/-}$ mice). The mice were established using the *Cre*-lox system to remove exons 1 and 2 of *A8* (Figure 1A). In the targeting construct, the neomycin gene is flanked by two *rox* sites that recombine to remove the neomycin (Neo) cassette, thus producing an allele with loxP sites flanking the first two exons of *A8*. Mice homozygous for the Floxed (*fl*) allele were used as controls for all experiments described in this paper unless otherwise stated, and are referred to as WT. *A8* was inactivated by crossing mice homozygous for the *fl* allele either with mice expressing *Cre* under control of the albumin promoter (Alb-*Cre*) (26) or with mice expressing *Cre* driven by the adiponectin promotor (Adipo-*Cre*) (27) to produce Ls-*A8*$^{-/-}$ mice and As-*A8*$^{-/-}$ mice, respectively. Both sexes transmitted the inactivated *A8* allele and the genotypes of the offspring conformed to the expected Mendelian ratios (Table S1). Litter sizes were similar in KO and WT mice (Table S2). Since A8 is not expressed in the fasting state, all experiments were performed in refed conditions unless otherwise stated.

The mean body weights of the C57BL/6N *A8*$^{-/-}$ mice were similar to those of WT controls at 9-10 weeks of age (Figure 1B). The mean total fat mass was significantly lower in the total *A8*$^{-/-}$ mice (3.0± 0.2 vs 1.7± 0.1 g), but not in the tissue-specific KO strains when compared to the WT animals (Figure 1B). Presumably the decreased fat mass in the total *A8*$^{-/-}$ mice is compensated by an increase in non-fat mass, although no significant differences in lean body mass were found between the strains. We compared the weights of selected other organs including the heart, skeletal muscle, spleen, and kidney and found no differences. In a group of older male mice (n=5/group, ages 10-15 weeks, age-matched), a small but significant decrease in mean body weight was seen in the *A8*$^{-/-}$ mice (25.2 ± 0.3 vs 23. ± 0.5, $P<0.04$) (Figure S1A).

This finding is consistent with data from our prior experiments using C57BL/6J *A8*$^{-/-}$ mice (28). Also consistent with our former observations, the body weights of the female *A8*$^{-/-}$ mice did not differ from the WT mice (Figure 1SB). The four groups of mice were housed in metabolic cages for a week to monitor food intake, activity level, VO_2 uptake and VCO_2 elimination. No differences in these parameters were seen among the four strains (Figure S1C). The As-*A8*$^{-/-}$ mice consumed slightly more food than the other strains in this experiment, but this difference was not apparent when the experiment was repeated. These results differ from our previous observations in *A8*$^{-/-}$ mice on a C57BL/6J background, which had increased VO_2 in the fed state (28). Genetic differences in fuel homeostasis between C57BL/6J and C57BL/6N have been documented previously (29), which may contribute to the differences in phenotype between the two strains of *A8*$^{-/-}$ mice.

Diet-induced hyperthermia in As-A8$^{-/-}$ *mice.* Previously, we found that C57BL/6J *A8*$^{-/-}$ mice maintained at room temperature (23°C) had higher core body temperatures than WT mice when fed *ad libitum*, but not when fasting (28). Similarly, no temperature differences were found between the 4 strains of mice after a 15 h fast. However, when measured 4 h after refeeding, rectal temperatures were significantly higher in the *A8*$^{-/-}$ and the As-*A8*$^{-/-}$ mice than in the WT animals (Figure 1C). The temperatures of the Ls-*A8*$^{-/-}$ mice did not differ from those of WT mice. Consistent with our published results on *A3*$^{-/-}$*A8*$^{-/-}$ mice, no increase in temperature in refed As-*A8*$^{-/-}$ mice was observed under conditions of thermoneutrality (Figure S1C). We concluded from this experiment that the increase in body temperature in the fed *A8*$^{-/-}$ is caused by a lack of A8 expression in adipose tissue.

Reduced fat pad mass and cell size in WAT of A8$^{-/-}$ *mice.* The fat pads were dissected from adjacent tissues and weighed. Representative fat pads from 12-week old male mice are shown in Figure 2A. The epididymal (Epi) fat pads from the *A8*$^{-/-}$ mice were visibly smaller and weighed significantly less than those from WT animals (Figure 2B), which is consistent with what was

seen in the *A3*$^{-/-}$*A8*$^{-/-}$ mice (28) and the *A8*$^{-/-}$ rat (30). The weights of the WAT-subcutaneous (SQ) fat were also lower in the *A8*$^{-/-}$ mice. Microscopic inspection of the fat pads revealed that cell size appeared to be smaller in both the WAT-Epi and –SQ fat from the *A8*$^{-/-}$ mice (Figure 2C). On average, adipocytes from both WAT depots were smaller than from the corresponding fat depots of WT controls (Figure 2D). We noted no differences among the strains in the morphology (Figure 2A) or histology (Figure 2C) of the inter-scapular brown adipose tissue (BAT) depots. The observation that the *A8*$^{-/-}$ mice, but not the tissue-specific *A8*$^{-/-}$ mice, have significantly smaller fat pads suggests that expression of A8 in either liver or WAT is sufficient to maintain normal TG accumulation in WAT.

Circulating A8 is liver-derived. To determine the relative contributions of liver and WAT to circulating A8, we immunoblotted plasma samples from WT, *A8*$^{-/-}$, Ls-*A8*$^{-/-}$, and As-*A8*$^{-/-}$, mice using an anti-A8 monoclonal antibody (Figure 3A, upper panel). An immunoreactive band migrating at the expected position of A8 (22 kDa) was observed in plasma of WT and As-*A8*$^{-/-}$ *mice.* No A8 protein was detected in the plasma of Ls-*A8*$^{-/-}$ or *A8*$^{-/-}$ mice. These data indicate that circulating A8 comes predominantly (and likely exclusively) from liver, with virtually no contribution from adipose tissue. It remains possible that some A8 synthesized in adipose tissue enters the circulation but is cleared so rapidly that it avoids detection in our analyses. Similar analysis of A3 in plasma revealed bands corresponding in size to full-length A3 (70 kDa) and the N- and C-terminal fragments of A3 (31 kDa and 38 kDa, respectively). The amount of the full-length protein was higher in the total *A8*$^{-/-}$ mice, as we previously observed (21), and in the Ls-*A8*$^{-/-}$ mice (Figure 3A, lower panel). Thus, A8 expression in the liver is associated with a reduction in circulating levels of full-length A3, but does not appear to alter the cleavage of A3.

To determine if higher levels of circulating A3 in *A8*$^{-/-}$ and *Ls-A8*$^{-/-}$ mice were due to increased expression of A3 in liver, we performed immunoblot analysis on liver lysates from animals that were perfused with saline before tissue collection. As expected, we observed no A8 in liver

lysates from the *A8*$^{-/-}$ and Ls-*A8*$^{-/-}$ mice (Figure 3B, upper panel). Two bands of the expected size for the unglycosylated (67 kDa) and fully glycosylated (70 kDa) forms of A3 were seen in all four groups of mice. Only faint bands corresponding to the N- and C-terminal fragments of A3 were observed. Expression levels of full-length A3 were higher in livers of *A8*$^{-/-}$ and Ls-*A8*$^{-/-}$ mice compared to WT or As-*A8*$^{-/-}$ mice (Figure 3B, lower panel). In the Ls-*A8*$^{-/-}$ mice, the 3-fold increase in full-length A3 protein was associated with a more modest 1.2-fold increase in A3 mRNA levels (Figure 3C). Thus, the higher levels of A3 protein in liver lysates and plasma of the *A8*$^{-/-}$ and Ls-*A8*$^{-/-}$ mice do not appear to be a consequence of differences in *A3* transcription. The results are consistent with a model in which A8 either promotes the intracellular degradation of A3 or accelerates clearance of A3 from the circulation. Additional experiments will be required to determine how A8 alters the expression of A3 in the liver and circulation.

As-*A8*$^{-/-}$ *mice have no immunodetectable A8 in WAT and BAT.* Immunoblot analysis of A8 in lysates from WAT-SQ and BAT in the fed state in the four strains of mice is shown in Figure 4A. No A8 was detected in the lysates from *A8*$^{-/-}$ and As-*A8*$^{-/-}$ mice. While we could not reliably detect A4 in tissues of mice using any of the available antibodies to A4, the levels of A4 mRNA were significantly lower in the WAT-SQ but not in the BAT of the *A8*$^{-/-}$ and Ls-*A8*$^{-/-}$ mice (Figure 4B). The lower levels of A4 mRNA in the WAT-SQ of these mice likely reflects the decrease in delivery of TG to WAT (21). A4 has been shown to be regulated by the transcription factor peroxisome proliferator-activated receptor-gamma (15), which is responsive to cellular fatty acid levels (31).

Absence of A8 in liver and adipose tissue has opposite effects on plasma TG levels. As we have shown previously, inactivation of A8 has little impact on fasting levels of plasma TG, cholesterol and nonesterified fatty acids (NEFA) (Figure 5A and 5B) [although a modest, but marginally significant (P=0.05) reduction in mean TG levels was seen in the A8 KO mice when compared to WT animals]. These are expected findings since A8 is expressed at very low levels

in fasting animals (11, 19, 20). Similarly, no changes in circulating fasting levels of cholesterol or glucose were seen in the tissue-specific A8 KO mice (Figure 5B, right).

In contrast to these findings, we observed significant differences in plasma TG levels between the groups after refeeding (Figure 5A, left). As expected (21), mean postprandial TG levels were significantly lower in *A8*$^{-/-}$ than in WT mice, whereas plasma levels of NEFA (and cholesterol) were similar in these two groups of animals. Levels of plasma TG were also dramatically reduced in the Ls-*A8*$^{-/-}$ mice. The reduction in mean levels of TG in the plasma of these mice was similar to those of the A*8*$^{-/-}$ mice (23.1 ± 1.1 versus 27.6 ± 2.5 mg/dL). These findings are consistent with the notion that liver-derived A8, together with A3, is responsible for inhibiting intravascular lipolysis in the refed state.

More surprising was the finding that plasma TG levels were increased in the fed As-*A8*$^{-/-}$ mice when compared to the WT animals (171.2 ± 8.3 versus 112.9 ± 7.3 mg/dL, $P<0.0001$). To determine if the increase in plasma TG levels in the As-*A8*$^{-/-}$ mice was caused by a decrease in intravascular lipolysis, we measured and compared heparin-releasable LPL activity among the strains. Four hours after eating, plasma was sampled (pre-heparin samples) prior to the administration of heparin (1 U/gm). Blood was collected 15 min after heparin administration and the plasma was subjected to heparin-affinity FPLC fractionation to separate hepatic lipase (HL) and LPL (32). Figure 5C (left) shows the lipolytic activities of the plasma fractions. Hepatic lipase activities were similar among the strains and did not change after heparin injection, as expected since HL circulates in plasma of mice (unlike humans) (33). Moreover, we showed previously that HL activity is not affected by A8 levels (21). In contrast to HL, LPL activities differed widely among the strains. LPL activity was increased to a similar extent in Ls-*A8*$^{-/-}$ and *A8*$^{-/-}$ mice when compared to As-*A8*$^{-/-}$ and WT animals. The increase in post-heparin plasma LPL activity in *A8*$^{-/-}$ mice was comparable to that seen in *A3*$^{-/-}$ mice, which is consistent with the hypothesis that the two proteins act together to inhibit LPL (Figure S2). In contrast to the

increase in post-heparin plasma LPL activity seen in Ls-*A8*$^{-/-}$ mice, As-*A8*$^{-/-}$ mice had an LPL activity that was similar to, or slightly lower than that seen in WT animals (Figure 5C, left).

To determine if the differences in LPL activity in our genetically modified mice are due to variations in the amount of enzyme on the endothelial surfaces, we compared levels of heparin-releasable LPL in the four strains. We incubated pooled post-heparin plasma with heparin-Sepharose beads, eluted the bound proteins, and then subjected the eluted proteins to immunoblotting (Figure 5C, right). In general, the relative abundance of LPL in each strain corresponded with the relative LPL activity (Figure 5C, left). The relative abundance of LPL was similar in Ls-*A8*$^{-/-}$ and *A8*$^{-/-}$ mice and higher than that observed in the WT or As-*A8*$^{-/-}$ mice. The slightly reduced amount and activity of LPL in the As-*A8*$^{-/-}$ mice compared to the WT mice may contribute to the increase in circulating TG levels seen in these animals after refeeding (Figure 5A).

To rule out the possibility that the increase in plasma TG levels in the As-*A8*$^{-/-}$ mice was due to an increase in VLDL-TG entry into plasma, we monitored the increase in plasma TG levels after inhibiting intravascular LPL using Triton WR 1339 (34). As expected, the mean plasma levels of TG were lower in the Ls-*A8*$^{-/-}$ mice at the start of the experiment. The rate of rise of TG levels was slower in the Ls-*A8*$^{-/-}$ mice than in the WT animals (5.57 mg/dL/min vs. 8.21 mg/dL/min, $P<0.01$). In contrast to these results, no significant differences were found in the rate of TG increase between the As-*A8*$^{-/-}$ (9.60 mg/dL/min) and WT mice (Figure S3).

A model of the effect of hepatic A8 expression on TG trafficking and substrate utilization in adipose tissue. To develop a framework for experimental testing, we revised our working model of how hepatic A8, together with A3, coordinate TG trafficking and utilization in the fed state (Figure 6A). In this model, feeding increases expression of A8 in liver. Liver-derived A8 forms a functional complex with A3 that inhibits LPL in oxidative tissues, thus reducing TG uptake in

those tissues. A greater proportion of circulating TG is now available for delivery to adipose tissue (Figure 6A, top panel). In the absence of A8, feeding fails to suppress LPL in oxidative tissues. Uptake of TG into oxidative tissues remains high and less TG is available for uptake by WAT (Figure 6A, second panel). Direct measurements of VLDL-TG delivery to tissues support this model (21). To compensate for the decreased delivery of TG to WAT, glucose uptake into WAT is greatly increased. The additional glucose provides the substrate for fatty acid and TG synthesis to maintain energy stores (21).

Based on our findings here, selective inactivation of A8 in liver would be predicted to disrupt delivery of TG to adipose tissue due to failure to inhibit intravascular lipolysis (Figure 6A, third panel). The reduction in TG delivery to WAT would result in an increase in both glucose uptake and endogenous synthesis of fatty acids in adipose tissue. Finally, in the As-*A8*$^{-/-}$ mice, TG trafficking would be expected to resemble that seen in the WT animals since both hepatic A3 and A8 are expressed in these animals (Figure 6A, lowest panel). The endocrine actions of A3/A8 on intravascular lipolysis ensure that sufficient TG is delivered to WAT to maintain tissue energy stores.

To test these predictions, we compared the ratio of C16:1, a fatty acid that is absent from the diet and must be synthesized endogenously (35), to C18:2 and C18:3, which are entirely diet derived, in several tissues. As expected, the ratio of endogenous/exogenous fatty acids increased in the WAT-Epi and WAT-SQ and to a lesser extent in BAT, but not in the liver of the *A8*$^{-/-}$ and Ls-*A8*$^{-/-}$ mice (Figure 6B). The increased ratio of endogenous/exogenous fatty acids was also noted in the circulating free fatty acid pool, of fasting animals, though absolute and relative abundance of C16:1 was much lower in plasma than in adipose tissue (note differences in y-axis scale). In contrast, the ratio of endogenous/exogenous fatty acids in the As-*A8*$^{-/-}$ mice was similar to that of WT animals in all tissues sampled. Thus, delivery of dietary fats to WAT is independent of adipose tissue-derived A8 in the fed state. As expected, the ratio of

endogenous/exogenous FAs in fasting plasma resembles that seen in the fed *A8*$^{-/-}$ and Ls-*A8*$^{-/-}$ mice (Figure S5).

We used RT-PCR (oligonucleotide sequences provided in Table S3) to measure levels of mRNAs encoding proteins involved in fatty acid synthesis and oxidation, glycolysis, beiging/ browning in WAT-SQ, -Epi, BAT and liver (Figure S4). The levels of mRNAs encoding enzymes involved in fatty acid synthesis were higher in the WAT of both the *A8*$^{-/-}$ and Ls-*A8*$^{-/-}$ mice. As shown previously, levels of SREBP-1c mRNA were increased in the WAT of *A8*$^{-/-}$ mice but not in our tissue-specific KO strains despite an increase in fatty acid synthesis gene expression in the Ls-*A8*$^{-/-}$ mice. Messenger RNA levels of another transcription factor that stimulates fatty acid synthesis, ChREBPβ (36), were significantly elevated in WAT of both the *A8*$^{-/-}$ and Ls-*A8*$^{-/-}$ mice and also increased, though not significantly in the As-*A8*$^{-/-}$ mice (Figure S4). We noted no differences in the mRNA levels of genes encoding proteins involved in fatty acid oxidation in WAT. Furthermore, UCP1 mRNA levels were not significantly altered in the 4 mouse strains in any of the tissues tested. None of the transcripts implicated in beiging/browning, except CIDEA and EVA1, differed among the strains (37). Levels of CIDEA and EVA1 transcripts were significantly higher in the *A8*$^{-/-}$ and Ls-*A8*$^{-/-}$ mice. Only minor changes were seen in the level of various hepatic mRNAs among the 4 strains of mice (Figure S4D). These patterns of RNA expression are consistent with the hypothesis that fatty acid synthesis is upregulated in the WAT of *A8*$^{-/-}$ and Ls-*A8*$^{-/-}$. Levels of the corresponding mRNAs were not increased in the livers of these mice. Therefore A3 and A8 secreted from the liver promote the efficient partitioning of fatty acids to WAT and thereby limit glucose uptake and *de novo* lipogenesis by this organ.

These observations beg the question as to the action of the adipose-specific A8 protein. One possibility is that A8 expression in adipocytes has local effects that include altering the synthesis or secretion of A4, the major regulator of LPL activity in WAT (38). Whereas mRNA levels of A4 and A8 are regulated reciprocally by fasting and feeding, Kroupa *et al.* showed that the turnover

of A4 protein is very slow in WAT from young rats treated with actinomycin D (39). After 6 h of treatment, levels of A4 mRNA were reduced by 93%, whereas levels of ANGPTL4 protein did not change. Thus, degradation of A4 appears to require the synthesis of new protein, possibly A8. We tested whether A8 promotes the degradation of A4 during the transition from fasting to refeeding, which would accelerate the activation of adipose tissue LPL in response to food intake. We tested this hypothesis by examining A4 synthesis and secretion in transiently transfected cultured cells expressing A4 and A8 (Figure 7A, top).

A8 expression reduces secretion of A4 from cultured cells. Recombinant A4 was expressed in the presence and absence of A8 in transiently transfected CHO-K1 cells. A doublet corresponding to the sizes of full-length, mature A4 (50 kDa) and the immature, deglycosylated precursor form of A4 (46 kDa) were seen in cells expressing A4 alone (Figure 7A, lanes 3 and 4) (22, 40). Expression of A4 together with A8 caused a reduction in the levels of A4, but not A8 in cell lysates (lanes 7 and 8). Cells were treated with heparin to analyze cell surface proteins. Bands corresponding to full-length A4 and A8 were seen in cells expressing either A4 or A8 alone after heparin treatment (Figure 7, lanes 11 and 12 or 13 and 14, respectively). However, in cells co-expressing A4 and A8, no heparin-releasable A4 protein was detected (lanes 15 and 16). This result is consistent with a scenario in which A8 expression promotes the intracellular degradation of A4.

To rule out the possibility that the absence of A4 on the surfaces of cells co-transfected with A8 was due to displacement of A4 by A8 on the cell surface, we examined the medium for the presence of A4. Bands of the expected size for the full-length and C-terminal domain of A4 were present in the medium of cells expressing A4 alone (lanes 19 and 20). Thus, a portion of the A4 undergoes catalytic cleavage during or after its secretion, as described previously (41). In contrast, when A8 and A4 were co-expressed, no full-length or cleaved A4 were detected in the medium (lanes 23 and 24). Thus, A8 expression dramatically reduces secretion of A4 from cells.

The levels of A8 were 50% lower in medium of cells co-expressing A8 and A4 than in cells expressing A8 alone (compare lanes 23 and 24 to lanes 21 and 22). Thus, A4 co-expression seemed to have a more tempered effect on secretion of A8.

Next, we examined the effect of A4 and A8 on LPL activity in the medium of CHO-K1 cells (Figure 7B). These cells have significant endogenous LPL activity, as indicated by the high lipase activity in cells expressing the control plasmid (column 1). Transfection with recombinant LPL plasmid further increased LPL activity (column 2). However, co-expression of LPL with A4, but not with A8, resulted in a dramatic reduction in LPL activity to almost undetectable levels, as had been observed previously (column 3 & 4, respectively) (42). Co-expression of A4 and A8 in cultured cells attenuated the inhibitory effect of A4 expression on lipase activity (column 5). Taken together, these results suggest that A8 interferes with secretion of A4 in cells, which serves to attenuate the LPL inhibitory action of A4. However, we cannot exclude the possibility that A8, either synthesized in the liver or adipose tissue, also acts in the subendothelial space.

To confirm that the observations made in cultured CHO cells resembled those seen in adipocytes, we used adenoviruses to express A4 and A8 in differentiated 3T3-L1 adipocytes (Figure 7C). The results were consistent with our findings in CHO-K1 cells: expression of recombinant A4 with A8 resulted in a significant reduction in A4 secretion. Conversely, A4 expression had little to no effect on A8 expression or secretion.

A8 physically interacts with A4 when co-expressed in cultured cells. Genetic ablation of A8 in mouse livers results in increased hepatic expression of A3 (Figure 3) while expression of A8 in differentiated 3T3-L1 adipocytes decreases expression of A4 (Figure 7C). These findings are consistent with a model in which interaction with A8 in the secretory pathway promotes the intracellular degradation of both A3 and A4. To test for interaction between A4 and A8, we expressed full-length recombinant epitope-tagged constructs of A4 (A4-myc), and A8 (A8-flag)

in QBI-293 cells and then immunoprecipitated A4 from the cell lysates (Figure 8A). In cells co-expressing A4-myc and A8, an anti-myc antibody precipitated both proteins. As expected, the anti-myc antibody failed to immunoprecipitate A8 from cells expressing A8 alone. Moreover, when the reverse experiment was performed and A8 was immunoprecipitated from cells, A4 was also pulled down with A8 (Figure 8A, right). Thus, A4 and A8 physically interact in cells expressing both proteins. We performed the same co-immunoprecipitation experiment in CHO-K1 cells and the results were similar (Figure S6).

Discussion

The major finding of this study is that the atypical angiopoietin-like protein, A8, has distinct functions in liver and adipose tissue. In both tissues, A8 acts by altering the activity of two canonical ANGPTLs: A3 in liver and A4 in adipose tissue. Selective inactivation of liver A8 resulted in mice with no circulating A8 (Figure 3A), high intravascular LPL activity, low plasma levels of TG, and increased endogenously synthesized fatty acids in WAT. These data indicate that essentially all circulating A8 originates in the liver, and that the postprandial inhibition of LPL activity in oxidative tissues, the major site of action of LPL, is mediated by a complex between liver-derived A8 and A3. Inactivation of A8 in adipose tissue had little to no effect on post-heparin plasma LPL activity and was associated with an increase rather than decrease in the level of circulating TG. Thus, A3 and A8 from liver, and A8 from adipose tissue use different mechanisms to control uptake and utilization of energy substrates by tissues in response to food intake.

The effects of liver-specific inactivation of A8 on plasma TG levels (Figure 5A) and on adipose fatty acid composition (Figure 6B) are remarkably similar to those seen in the *A8*$^{-/-}$ mice (7). Other than promoting intravascular LPL inhibition (Figure 5), A8 expression in liver is also associated with a reduction in A3 secretion. WT and As-*A8*$^{-/-}$ mice had lower levels of full-length A3 (but not the cleaved fragments of A3) in both plasma and liver lysates than either the Ls-*A8*$^{-/-}$ or total *A8*$^{-/-}$ mice (Figure 3A and 3B). By reducing A3 secretion, A8 may indirectly alter the activity of another lipase, endothelial lipase (EL) (43) since A3 inhibits EL (44) and this activity does not require A8.

Full-length A3 levels were increased in the plasma and liver of the *A8*$^{-/-}$ and the Ls-*A8*$^{-/-}$ mice, without an increase of similar magnitude in A3 mRNA, suggesting that A8 expression is associated with reduced secretion of A3 from the liver. Very low levels of C-ter or N-ter

fragments of A3 were visible in liver lysates, yet levels of the two fragments in plasma were similar among the 4 strains (Figure 3). These results are consistent with cleavage of A3 occurring after its secretion from liver. Additional experiments will be required to determine why levels of the A3 fragments do not differ between the strains of mice.

Unlike the effect of A3 on EL, which does not require A8, the inhibitory effect of A3 on LPL activity is markedly enhanced in the presence of A8 (25). The results of *in vitro* studies suggest that A8, rather than A3, mediates the physical interaction between the A3/A8 complex and LPL (25). Disruption of the LPL binding site of A3 does not attenuate the inhibitory effect of the A3/A8 complex on LPL. Although detailed biophysical studies of the interaction between the A3/A8 complex and LPL have not been performed, we would predict that A3/A8 binding to LPL results in degradation of the protein. Consistent with this prediction, the amount of LPL in post-heparin plasma of *A3*$^{-/-}$ and *A8*$^{-/-}$ mice was increased to a similar extent and was proportional to the increase in LPL activity (Figure S2). Moreover, A8 from liver, but not from adipose tissue, confers this effect on LPL (Figure 5C).

Although the Ls-*A8*$^{-/-}$ mice recapitulate the intravascular phenotype of the *A8*$^{-/-}$ mice, inactivation of A8 in the liver alone does not cause a reduction in body weight or fat pad mass (Figure 1B and 2B). This finding implies a role for A8 expressed in adipose tissue in the maintenance of TG stores. How is this accomplished? In contrast to hepatocytes, adipocytes do not appear to contribute to the A8 plasma pool (Figure 3A). The As-*A8*$^{-/-}$ mice have similar, albeit slightly lower post-heparin LPL levels and activity (Figure 5C), which may contribute to the higher plasma TG levels (Figure 5A) seen in these animals when compared to WT mice. Our data suggest that A8 in adipose tissue antagonizes the inhibitory effect of A4 on LPL activity. A8 synthesis (and A4 inhibition) in adipose tissue in the early fasting-refeeding transition would increase LPL activity in adipose tissue and enhance the rate at which TG stores are replenished, thus better preparing the animal for the next fast (Figure 8B).

The accumulation of C16:1 and depletion of C18:2 in WAT of A8-/-mice is consistent with our previous finding that inactivation of A8 prevents the postprandial increase in the uptake of circulating TGs that replenishes WAT in WT animals. A similar elevation in the ratio of C16:1 to C18:2/18:3 was seen in WAT from the Ls-*A8*$^{-/-}$ mice, but not in As-*A8*$^{-/-}$ mice. These data indicate that the uptake of circulating TG-fatty acids by WAT is controlled by endocrine actions of A8 from the liver, rather than by the adipocytes themselves. Despite similar increases in C16:1 to C18:2/18:3 ratios, the mass of the epididymal fat pads was markedly reduced in A8-/- mice, but not in the Ls-*A8*$^{-/-}$ mice. Thus, the increases in glucose uptake and de novo fatty acid synthesis that drive the changes in FA composition in the WAT of these animals is sufficient to preserve WAT in the Ls-*A8*$^{-/-}$ mice but not in the *A8*$^{-/-}$ mice. Liver-specific -*A8*$^{-/-}$ mice resemble the adipose tissue-specific LPL KO in that they have both increased de novo lipogenesis in adipose tissue, as reflected by the changes in fatty acid composition (45). Taken together, these data indicate that expression of A8 either in liver or in adipose tissue is sufficient to preserve WAT mass in mice.

Figure 8B depicts our current model of LPL regulation by A4 and A8 in WAT. In fasting animals, the levels of A4 in WAT are high, whereas those of A8 are very low (Figure 8B, top). A4 is a potent inhibitor of LPL: prior studies in cultured cells showed that co-expression of recombinant A4 and LPL promotes the intracellular degradation of LPL, although the mechanism by which this is accomplished remains unclear (42). Consequently, LPL activity is low in WAT during fasting, causing circulating TG to bypass WAT in favor of oxidative tissues where LPL activity is high.

Conversely, A8 expression is induced upon feeding (Figure 8B, bottom). In this situation, A8 physically interacts with A4 in adipocytes, leading to its degradation. This finding is consistent with the data of Kovrov et al. (14) who reported that purified recombinant A8 can form complexes with the N-terminal domain of A4 if the proteins are refolded together from their

denatured state. Under those conditions, A8 decreased the inhibitory effect of A4 on LPL activity by about 50%. If A8 has the same effect on A4 secretion *in vivo* in adipose tissue as it does in cultured adipocytes (Figure 7C), then A8 expression in WAT would reduce the LPL inhibitory effect of A4 and increase LPL activity in adipose tissue. In short, A8 would act locally in WAT to enhance the uptake of TG into adipocytes upon feeding, leading to a more rapid repletion of energy stores. Based on this model, we predict that the trafficking of LPL is similar in fasting WT and As-*A8*$^{-/-}$ mice (Figure 8B, top) since A4 promotes intracellular degradation of LPL, resulting in less LPL in the intravascular space. In both strains, circulating TG would largely evade hydrolysis in WAT and be preferentially delivered to oxidative tissues. We provide evidence that A8 within adipocytes acts inside the cell to attenuate the inhibitory effect of A4 on LPL activity. However, we cannot exclude a potential action of A8 in the subendothelial space too. Since we show that A8 physically interacts with A4 it is also plausible that circulating A8 could block the extracellular endothelial cell-associated effects of A4. Taken together, these findings are compatible with a model in which A8 has a dual role that is dependent on its site of expression, and on its stoichiometric relationships with A3 and A4. In liver, A8 activates A3 to form an A3/A8 heterodimer. The A3/A8 heterodimer acts as an endocrine factor that mediates postprandial re-routing of TG from oxidative tissues to adipose tissue. In adipose tissue, A8 interacts instead with A4 and functions in an autocrine or paracrine fashion to facilitate energy storage in adipocytes.

The most perplexing phenotypes seen in the tissue-specific *A8*$^{-/-}$ mice are the increases in plasma TG and in body temperature in the As-*A8*$^{-/-}$ mice when compared to WT animals (Figure 1C and Figure 5A). The increase in plasma TG in As-*A8*$^{-/-}$ mice cannot be explained by previous models from our laboratory or others (21), which assumed that a single pool of circulating A8 acts together with A3 to inhibit LPL in the circulation. If adipose tissue does not contribute to the intravascular pool of A8 (Figure 3), why does inactivating A8 in that tissue cause an increase in

plasma TG (Figure 5A)? We have ruled out the possibility that inactivating A8 in mice increases plasma TGs by increasing VLDL-TG secretion (Figure S3). It may be that the absence of A8 in adipocytes results in greater A4 activity and decreased secretion of LPL, and hence increase in TG in the fed state. Additional experiments will be required to test this hypothesis.

Basic mechanistic questions remain even for A4, the best studied of the three ANGPTL proteins. The Neher laboratory proposed that A4 binds the lid domain of LPL and occludes access to the catalytic site (46). In this model, inhibition of LPL activity is reversible and does not involve denaturation or dissociation of the enzyme. The Olivecrona laboratory reported that A4 promotes irreversible dissociation of dimeric LPL into catalytically inactive monomers (38). Inactivation of LPL occurred at sub-stoichiometric ratios of A4, which was not consumed (38). Using deuterium exchange, Mysling *et al.* (47) also found that A4 inactivates LPL at sub-stoichiometric ratios and that binding of A4 to LPL results in irreversible unfolding of the protein. Studies by the same group showed that A3 had a similar but much weaker effect (47). Although further biochemical studies will be required to elucidate the specific mechanism by which A3/A8 inhibits LPL, the increase in both the activity and the amount of LPL in post-heparin plasma from A8 knockout mice indicates that A3/A8 binding to LPL results in depletion of the enzyme from the capillary endothelial surfaces. These data favor a model in which A3/A8 binding to LPL results in irreversible inactivation, possibly via unfolding of LPL (47) and degradation of the enzyme.

A8$^{-/-}$ mice are hyper-metabolic for reasons that remain to be elucidated (28). These effects were more pronounced in the *A3*$^{-/-}$*A8*$^{-/-}$ mice, but were absent in the *A3*$^{-/-}$ mice (28). We noted differences between the C57BL/6J background of *A8*$^{-/-}$ mice we studied previously and the *A8*$^{-/-}$ mice used in the experiments described in this paper, which were in a different substrain of C57BL/6 (C57BL/6N). On a C57BL/6J background, the mice had an increase in VO_2 consumption, which we did not see in the C57BL/6N mice (Figure S1C). The reason for these

differences may be due to the well documented differences in substrate utilization between these two strains of mice (29). Alternatively, the differences may be due to environmental factors that have yet to be identified.

An increased body temperature in response to eating was apparent in both strains of mice. In both strains, no difference in body temperature were apparent in the fasting state, but only after refeeding (Figure 1C) and inly if the mice were maintained at a temperature lower than thermoneutrality (Figure S1C). Previously, we showed that we could normalize the body temperature of *A3*$^{-/-}$*A8*$^{-/-}$ mice by inhibiting the β3-adrenergic receptor, which is only expressed in adipocytes (48). These results suggested that the effect of A8 inactivation on body temperature was due to A8 expression in adipose tissue,

not the brain function. Here we did not see any postprandial increase in body temperature in Ls-*A8*$^{-/-}$ animals, which further implicates A8 expression in in the adipose tissue being responsible for changes in body temperature. Our data do not implicate A8 expression in BAT as a major contributor to the phenotypes observed in our tissue-specific KO mice. These observations are consistent with our previous findings (7, 28). We showed that A8 physically interacts with A4 (Figure 8A) and reduces its secretion in cultured adipocytes (Figure 7C). Thus, absence of A8 in adipose tissue would be expected to cause an increase in the secretion of A4. A4 undergoes catalytic cleavage, releasing the N- and C-terminal fibrinogen-like domains. The C-terminal fibrinogen-like domain of A4 has been shown to activate the β3-adrenergic receptor signaling pathway (49), which we showed previously plays a critical role in the hyperthermia associated with A8 inactivation (28). Additional studies will be required to determine how A8 suppresses postprandial and temperature-related increases in body temperature.

Methods

Mice. The genetically-modified mice used in these studies were in a C57BL/6NTac genetic background. The albumin-*Cre* transgenic mice were obtained from Jackson Laboratories and were on C57BL/6N background (*https://www.jax.org/strain/018961*). The adiponectin-Cre mice were provided by Philipp Scherer (UTSW) and backcrossed 7 generations with C57BL/6N from Charles River (*https://www.criver.com/products-services/find-model/c57bl6-mouse?region=3611*) prior to being bred to the genetically modified A8 mice. The *fl/fl* mice were obtained from Regeneron Pharmaceuticals. To generate hepatocyte [referred to as liver-specific, (Ls)-$A8^{-/-}$ mice] and adipocyte [adipose tissue-specific (As-$A8^{-/-}$) mice], the *fl/fl* mice were crossed with Alb-*Cre* and Adipo-*Cre* mice, respectively. The $A8^{-/-}$ mice were generated as described (11, 21, 50) and backcrossed with C57BL/6N mice for 7 generations. Mice were maintained at 21–23 °C on a 12-h dark/light cycle (lights on: 6:00 AM–6:00 PM), and fed a rodent chow diet (Teklad Global, 16% protein). For all experiments, unless otherwise stated, the feed/fast cycles of the mice were synchronized for 3 days by removing food during the night for 15 h (6:00 PM–9:00 AM) and providing food at 9:00 AM. Samples were collected after the 15 h fast (fasting) or 4 h after the mice were provided food (fed).

Mice were placed in metabolic cages (LabMaster System; TSE Systems) for 3 days prior to measuring food intake and physical activity, which were monitored for 1 min every 50 min for 4 days. Indirect calorimetry was performed to measure VO_2 consumption and VCO_2 output. Measurements of body composition, including fat mass, lean tissue mass, free water, and total body water were performed in non-anesthetized mice using NMR (Bruker Minispec MQ10), as previously described (7).

Rectal temperatures were measured using a thermocouple thermometer probe (BAT-7001H; Physitemp Instrument Inc.) that was inserted at least 1.5 cm into the rectum.

Biochemical Analysis. Blood was collected from tail veins in citrate-EDTA tubes and plasma was isolated by centrifugation at 2,000 x *g* for 10 min at 4 °C. Plasma levels of TG and cholesterol were measured using Infinity series kits (Thermo Scientific Inc.). Nonesterified fatty acid levels were measured in duplicate or triplicate using the HR Series NEFA-HR Kit (Fujifilm Wako Diagnostics). Results were obtained using the Synergy Neo2 plate reader (BioTeck Instruments). Plasma glucose levels were measured using Coultour Blood Glucose Monitoring System (Bayer).

For fatty acid analysis of tissues, lipids were extracted from the blood (51) of the fasting and refed animals, derivatized to form methyl esters and separated by gas/liquid chromatography using a Hewlett Packard 6890 Series GC system. The identity of the fatty acid methyl ester was determined by comparing the retention times with fatty acid standards (GLC-744; NU-Chek Prep). The abundance of each fatty acid was determined from the peak intensity and the internal standard. Fatty acid profiles were generated using a modified GC-MS method, as previously described (52).

*Cell Culture***.** 3T3-L1 murine fibroblasts (provided by the Department of Molecular Genetics, UTSW, TX) were propagated and differentiated to adipocytes as described (53).

CHO-K1 cells (Chinese Hamster Ovary epithelial cells, provided by the Department of Molecular Genetics, UTSW, TX) were cultured in DMEM/F12 with FBS (10%) and penicillin-streptomycin (1%). Myc-tagged human A4, Flag-tagged human A8, V5/His6-tagged human LPL, and empty vector pcDNA3.1 were transfected into CHO-K1 cells according to the manufacturer's instruction (Fugene® 6 Transfection Regent). After 48 h, the cell culture medium was collected and LPL activity was assayed. Cells were first washed with cold PBS once and then incubated on ice with 0.5 ml of PBS + heparin (50 U/ml) for 20 min on ice to release surface-bound LPL. The heparin-released fraction was removed and assayed for lipase activity. Cells were

suspended in 300 µL of 20 mM Tris, pH 7.5, 150 mM NaCl, and 5U/ml heparin and then homogenized by sonication for 3 X 5 sec. After removal of insoluble material, the supernatant was loaded onto SDS-PAGE and subjected to Western blotting.

QBI-293 cells (human kidney cells, provided by the Department of Molecular Genetics, UTSW, TX) were cultured in DMEM with FBS (5%) and penicillin-streptomycin (1%). The protocol for transfection of QBI-293 cells was identical to that described for CHO-K1 cells.

Immunoprecipitation. QBI293 cells were cultured in 100-mm dishes and e transfected with myc-tagged human A4, Flag-tagged human A8, and empty vector pcDNA3.1. Cells were collected 48 h post-transfection and suspended in 1 ml of RIPA buffer (25 mM Tris-HCl pH 7.6, 150 mM NaCl, 1% NP-40, 1% sodium deoxycholate, 0.1% SDS) plus protease inhibitor. The cells were homogenized by sonication for 3 X 5 sec. After removal of insoluble material, the protein concentration was quantified by BCA (Bicinchoninic Acid Assay). Lysates containing 800 µg total protein were incubated with 20 µl of pre-washed Anti-FLAG M2 magnetic beads or anti-Myc magnetic beads for 3 h at 4°C. For A4 immunoprecipitation, Anti-Myc beads were washed 3 times with RIPA buffer and resolved in 50 µl of protein loading buffer. A total of 20 µl was loaded onto SDS-PAGE and subjected to immunoblotting. For A8 immunoprecipitation, Flag beads were washed 3 X with RIPA buffer and then incubated with 50 µl of 1 mg/ml 3x Flag peptides in TBS buffer (25 mM Tris-HCl pH 7.5, 150 mM NaCl) for 20 min at room temperature. A total of 20 µl of the total elution was loaded onto SDS-PAGE and analyzed by immunoblotting.

SDS-PAGE and Immunoblot Analysis. Tissues were collected from mice after a15 h fast or after refeeding for 4 h. The tissues were snap-frozen in liquid nitrogen and stored at -80°C. Lysates of WAT were prepared using the Minute™ Total Protein Extraction Kit for Adipose Tissues/Cultured Adipocytes according to the manufacturer's protocol (Invent Biotechnologies). Protein concentrations were determined using the Bio-Rad Bradford protein assay according to

the manufacturer's protocol. Mouse plasma was diluted 10-fold in 0.9% NaCl and then incubated at 85 °C for 3 min in Laemmli SDS reducing sample buffer (375 mM Tris-HCl, 9% (W/V) SDS, 50% glycerol, 9% β-mercaptoethanol, 0.03% bromophenol blue, pH 6.8). A total of 10 µL of diluted plasma was size-fractionated on a 15% SDS-polyacrylamide gel at 125 V and transferred to nitrocellulose (GE Healthcare). Membranes were incubated in PBST buffer (1X PBS, 0.1% Tween 20, pH 7.4) with 5% fat-free milk (Carnation) for 60 min at room temperature before overnight incubation at 4°C with antibodies diluted in PBST buffer plus 5% fat-free milk. The following polyclonal Abs were used for immunoblotting: rabbit anti-fibronectin Ab (Abcam, Ab2413, 1:5000), goat anti-mouse A3 Ab (AF136, R&D Systems, 1:1,000), and rabbit anti-calnexin Ab (Fisher Scientific, ADI-SPA-860-F, 1:3000). Mouse anti-A8 mAb (IgG-19H4, 1:500) was produced by injecting New Zealand Black mice seven times with full-length recombinant mouse A8. Positive clones were screened by ELISA, confirmed by immunoblotting, and subcloned by serial dilution. The final subclone was expanded and the cell culture supernatant purified on a Protein G (4 Fast Flow) gravity column.

After incubation with the antibody, membranes were washed 3 times for 10 min in PBST buffer before adding horseradish peroxidase-conjugated goat anti-mouse or anti-rabbit IgG (1:10,000) (Jackson Immuno- Research) in PBST plus 1.25% fat-free milk. Following a 60 min incubation at room temperature, membranes were washed with PBST and visualized using SuperSignal-enhanced chemiluminescence (Pierce) prior to being exposed to F-BX810 Blue X-Ray films (Phoenix Research Products). Band intensities were analyzed using LI-COR Image Studio™ Lite version 5.2.5. For detection of human A4 and A8 in cell lysates and media, rabbit polyclonal anti-human A8 (149D) was used. 149D Ab was produced by injecting rabbits ten times with His-tagged full-length protein in Freund's adjuvant.

For detection of LPL and HL in mouse plasma, pooled plasma samples (10 µl) were diluted in 500 µl of PBS. The diluted samples were incubated with heparin beads (20 µl) for 2 h. The

heparin bead-bound proteins were then subjected to SDS-PAGE and western blotting. The following Abs were used for immunoblotting: rabbit polyclonal anti-LPL polyclonal Ab (R&D Systems) and rabbit anti-mouse HL polyclonal antibody (LIPC, LSBio). Ponceau staining was used for detection of proteins in the media (Sigma Aldrich).

Expression of Recombinant Human A4 and A8 in Differentiated Murine Adipocytes (3T3-L1 cells). Recombinant adenoviruses (1 X 10^9 viral particles) expressing human A4 and A8 (11, 54) were used to infect differentiated adipocytes. The medium was replaced with serum-free medium 2 h post infection. After 24 h, the medium was collected and subjected to centrifugation for 5 min (3,500 x g, RT). The supernatant was concentrated 40-fold using Centrifugal Filters (Amicon Ultra, 10 mL–10 K; Millipore). Cell lysates were prepared using the Minute™ Total Protein Extraction Kit for Adipose Tissues/Cultured Adipocytes according to the manufacturer's protocol (Invent Biotechnologies).

Real-Time PCR Assay of mRNA Levels. Total RNA was extracted from tissues (n=4-6 per genotype) using Qiagen RNeasy Plus Universal mini Kit (73404). Complementary DNA was obtained from 2 µg of total RNA using TaqMan (Applied Biosystems) with random hexamer primers. Oligonucleotides specific for each transcript (Table S3) were used to amplify from total RNA by qPCR in 2 x SYBR Master Mix (Applied Biosystems) according to the manufacturer's instructions. Messenger RNA levels were normalized to levels of mouse 36B4 (liver), cyclophillin (WAT-Epi and BAT) and HPRT (WAT-SQ) transcripts. For each transcript, the mean level of the WT animals was set to 1.

Intravascular Lipase Activity. Heparin-Sepharose chromatography was performed using an ÄKTA-purifier system (GE Healthcare). Briefly, a HiTrap Heparin HP 1-ml column was equilibrated with buffer A [20 mM TrisCl, 0.15 M NaCl, 1% (w/v) BSA, and 20% (v/v) glycerol]. A total of 250 µl of plasma pooled from 5 mice was applied to the column. The column was

washed with buffer A and eluted with a linear gradient of NaCl (from 0.15 to 2.0 M) in buffer A (38). Lipoprotein lipase activity was measured using a commercial LPL assay kit (STA-610, Cell BioLabs, Inc.). Adipose tissue (100 mg) or other tissues (50 mg) were homogenized in 1 ml of cold Buffer A (20 mM Tris, pH 7.5, 150 mM NaCl) and then centrifuged for 10 min at 10,000 x g. After incubation of tissue lysate or diluted plasma (10 μl) with reagents from the assay kit according to the manufacturer's instruction, the fluorescence signal (excitation in 480–485 nm and emission in the 515–525 nm) was read and recorded with a fluorescence microplate reader (Synergy Neo2, BioTek Instruments). LPL activity was calculated following instructions provided in the kit.

Histology. Following an overnight fixation in paraformaldehyde (4%), tissues were washed with PBS and processed for paraffin embedding. Tissues were sectioned to a thickness of 5 μm and stained with H&E as described previously (28). Stained sections were examined using light microscopy (20x). For each group, tissues from 5-6 mice were collected and stained. Representative images are shown.

Rectal Temperature, Indirect Calorimetry and Body Composition Measurements. We recorded rectal temperatures in fasting and refed mice as described above. For measurements of energy homeostasis, mice were acclimated to the new environment for 3 days before data collection. Measurements of body composition, including fat mass, lean tissue mass, free water, and total body water were performed in non-anesthetized mice by NMR (Bruker Minispec MQ10).

VLDL-TG Secretion Measurements. Mice were injected with a bolus Triton WR-1339 (500 mg/kg) (Tyloxapol; Sigma-Aldrich) via the tail vein. Blood was collected from the tail vein at several time points and plasma levels of TG were determined using a colorimetric assay (Infinity Series Kit, Thermo Scientific).

Statistical Analysis. All results are expressed as mean ± SEM. Differences among groups were analyzed by unpaired two-tailed Student's *t* test, one-way ANOVA followed by Dunnett`s multiple comparison test or two-way ANOVA for multiple comparisons. Analyses were performed using GraphPad Prism version 8.1.1 (GraphPad Software). Power calculations were performed using available online sources (*http://www.biomath.info/power/ttest.htm*). The sample sizes used in indirect calorimetry studies (n=7 mice/group) were estimated to provide 90% power to detect differences in VO_2 and VCO_2 of 1.5 SD (equivalent to 300 ml/kg/h). For rectal temperature measurements, a sample size of 7 was estimated to 90% power to detect a difference in the means of 0.6°C. For all experiments, a *P* value of <0.05 was considered statistically significant.

Study approval. All protocols were approved by the Institutional Animal Care and Use Committee of the University of Texas Southwestern Medical Center.

Authors Contributions

FO, HC, JCC, and HHH designed the experiments and FO and HC performed the experiments. SB and VG contributed new reagents/analytic tools; FO, HC, JCC, and HHH analyzed data; FO, HC, SB, GV and JCC, and HHH wrote the paper.

Acknowledgements

We thank Christina Zhao, Liangcai Nie, Fang Xu, Tommy Hyatt, Maritza Thomas, and Lisa Beatty for technical support, Julia Kozlitina for statistical advice and Fabienne Elwood for administrative support. JCC and HHH were supported by grants from the National Institutes of Health (5 PO1 HL20948).

References

1. Gofman JW, Jones HB, Lindgren FT, Lyon TP, Elliott HA, and Strisower B. Blood lipids and human atherosclerosis. *Circulation.* 1950;2(2):161-78.
2. Gage SH, Fish, P.A. Fat digestion, absorbtion and assimilation in man and animals as determined by the dark-field microscope and a fat-soluble dye. *Am J Anat.* 1924;34(1).
3. Hahn PF. Abolishment of alimentary lipemia following injection of heparin. *Science.* 1943;98(2531):19-20.
4. Korn ED. Clearing factor, a heparin-activated lipoprotein lipase. I. Isolation and characterization of the enzyme from normal rat heart. *J Biol Chem.* 1955;215(1):1-14.
5. Kuwajima M, Foster DW, and McGarry JD. Regulation of lipoprotein lipase in different rat tissues. *Metabolism.* 1988;37(6):597-601.
6. Lithell H, Boberg J, Hellsing K, Lundqvist G, and Vessby B. Lipoprotein-lipase activity in human skeletal muscle and adipose tissue in the fasting and the fed states. *Atherosclerosis.* 1978;30(1):89-94.
7. Wang Y, et al. Hepatic ANGPTL3 regulates adipose tissue energy homeostasis. *Proc Natl Acad Sci U S A.* 2015;112(37):11630-5.
8. Bergo M, Wu G, Ruge T, and Olivecrona T. Down-regulation of adipose tissue lipoprotein lipase during fasting requires that a gene, separate from the lipase gene, is switched on. *J Biol Chem.* 2002;277(14):11927-32.
9. Koishi R, et al. Angptl3 regulates lipid metabolism in mice. *Nat Genet.* 2002;30(2):151-7.
10. Kersten S. Physiological regulation of lipoprotein lipase. *Biochim Biophys Acta.* 2014;1841(7):919-33.
11. Quagliarini F, et al. Atypical angiopoietin-like protein that regulates ANGPTL3. *Proc Natl Acad Sci U S A.* 2012;109(48):19751-6.
12. Lee EC, et al. Identification of a new functional domain in angiopoietin-like 3 (ANGPTL3) and angiopoietin-like 4 (ANGPTL4) involved in binding and inhibition of lipoprotein lipase (LPL). *J Biol Chem.* 2009;284(20):13735-45.
13. Shan L, et al. The angiopoietin-like proteins ANGPTL3 and ANGPTL4 inhibit lipoprotein lipase activity through distinct mechanisms. *J Biol Chem.* 2009;284(3):1419-24.
14. Kovrov O, Kristensen KK, Larsson E, Ploug M, and Olivecrona G. On the mechanism of angiopoietin-like protein 8 for control of lipoprotein lipase activity. *J Lipid Res.* 2019;60(4):783-93.
15. Kersten S, et al. Characterization of the fasting-induced adipose factor FIAF, a novel peroxisome proliferator-activated receptor target gene. *J Biol Chem.* 2000;275(37):28488-93.
16. Kersten S. Regulation of lipid metabolism via angiopoietin-like proteins. *Biochem Soc Trans.* 2005;33(Pt 5):1059-62.
17. Conklin D, et al. Identification of a mammalian angiopoietin-related protein expressed specifically in liver. *Genomics.* 1999;62(3):477-82.
18. Ge H, et al. Differential regulation and properties of angiopoietin-like proteins 3 and 4. *J Lipid Res.* 2005;46(7):1484-90.
19. Ren G, Kim JY, and Smas CM. Identification of RIFL, a novel adipocyte-enriched insulin target gene with a role in lipid metabolism. *Am J Physiol Endocrinol Metab.* 2012;303(3):E334-51.
20. Zhang R. Lipasin, a novel nutritionally-regulated liver-enriched factor that regulates serum triglyceride levels. *Biochem Biophys Res Commun.* 2012;424(4):786-92.

21. Wang Y, et al. Mice lacking ANGPTL8 (Betatrophin) manifest disrupted triglyceride metabolism without impaired glucose homeostasis. *Proc Natl Acad Sci U S A.* 2013;40(110):16109-14.
22. Ge H, Yang G, Huang L, Motola DL, Pourbahrami T, and Li C. Oligomerization and regulated proteolytic processing of angiopoietin-like protein 4. *J Biol Chem.* 2004;279(3):2038-45.
23. Koliwad SK, et al. Angiopoietin-like 4 (ANGPTL4, fasting-induced adipose factor) is a direct glucocorticoid receptor target and participates in glucocorticoid-regulated triglyceride metabolism. *J Biol Chem.* 2009;284(38):25593-601.
24. Gray NE, Lam LN, Yang K, Zhou AY, Koliwad S, and Wang JC. Angiopoietin-like 4 (Angptl4) protein is a physiological mediator of intracellular lipolysis in murine adipocytes. *J Biol Chem.* 2012;287(11):8444-56.
25. Haller JF, et al. ANGPTL8 requires ANGPTL3 to inhibit lipoprotein lipase and plasma triglyceride clearance. *J Lipid Res.* 2017;58(6):1166-73.
26. Postic C, et al. Dual roles for glucokinase in glucose homeostasis as determined by liver and pancreatic beta cell-specific gene knock-outs using Cre recombinase. *J Biol Chem.* 1999;274(1):305-15.
27. Wang ZV, Deng Y, Wang QA, Sun K, and Scherer PE. Identification and characterization of a promoter cassette conferring adipocyte-specific gene expression. *Endocrinology.* 2010;151(6):2933-9.
28. Banfi S, Gusarova V, Gromada J, Cohen JC, and Hobbs HH. Increased thermogenesis by a noncanonical pathway in ANGPTL3/8-deficient mice. *Proc Natl Acad Sci U S A.* 2018;115(6):E1249-E58.
29. Rendina-Ruedy E, et al. A comparative study of the metabolic and skeletal response of C57BL/6J and C57BL/6N mice in a diet-induced model of Type 2 diabetes. *J Nutr Metab.* 2015;2015 (758080): 1-13.
30. Izumi R, et al. CRISPR/Cas9-mediated Angptl8 knockout suppresses plasma triglyceride concentrations and adiposity in rats. *J Lipid Res.* 2018;59(9):1575-85.
31. Forman BM, et al. 15-Deoxy-delta 12, 14-prostaglandin J2 is a ligand for the adipocyte determination factor PPAR gamma. *Cell.* 1995;83(5):803-12.
32. Garfinkel AS, and Schotz MC. Separation of molecular species of lipoprotein lipase from adipose tissue. *J Lipid Res.* 1972;13(1):63-8.
33. Dallinga-Thie GM, et al. Appraisal of hepatic lipase and lipoprotein lipase activities in mice. *J Lipid Res.* 2007;48(12):2788-91.
34. Millar JS, Cromley DA, McCoy MG, Rader DJ, and Billheimer JT. Determining hepatic triglyceride production in mice: comparison of poloxamer 407 with Triton WR-1339. *J Lipid Res.* 2005;46(9):2023-8.
35. Palmquist DL, St-Pierre N, and McClure KE. Tissue fatty acid profiles can be used to quantify endogenous rumenic acid synthesis in lambs. *J Nutr.* 2004;134(9):2407-14.
36. Herman MA, et al. A novel ChREBP isoform in adipose tissue regulates systemic glucose metabolism. *Nature.* 2012;484(7394):333-8.
37. Seale P, et al. Transcriptional control of brown fat determination by PRDM16. *Cell Metab.* 2007;6(1):38-54.
38. Sukonina V, Lookene A, Olivecrona T, and Olivecrona G. Angiopoietin-like protein 4 converts lipoprotein lipase to inactive monomers and modulates lipase activity in adipose tissue. *Proc Natl Acad Sci U S A.* 2006;103(46):17450-5.
39. Kroupa O, et al. Linking nutritional regulation of Angptl4, Gpihbp1, and Lmf1 to lipoprotein lipase activity in rodent adipose tissue. *BMC Physiol.* 2012;12(13.
40. Dijk W, Ruppert PMM, Oost LJ, and Kersten S. Angiopoietin-like 4 promotes the intracellular cleavage of lipoprotein lipase by PCSK3/furin in adipocytes. *J Biol Chem.* 2018;293(36):14134-45.

41. Lei X, et al. Proteolytic processing of angiopoietin-like protein 4 by proprotein convertases modulates its inhibitory effects on lipoprotein lipase activity. *J Biol Chem.* 2011;286(18):15747-56.
42. Dijk W, Beigneux AP, Larsson M, Bensadoun A, Young SG, and Kersten S. Angiopoietin-like 4 promotes intracellular degradation of lipoprotein lipase in adipocytes. *J Lipid Res.* 2016;57(9):1670-83.
43. McCoy MG, Sun GS, Marchadier D, Maugeais C, Glick JM, and Rader DJ. Characterization of the lipolytic activity of endothelial lipase. *J Lipid Res.* 2002;43(6):921-9.
44. Jin W, Fuki IV, Seidah NG, Benjannet S, Glick JM, and Rader DJ. Proprotein convertases [corrected] are responsible for proteolysis and inactivation of endothelial lipase. *J Biol Chem.* 2005;280(44):36551-9.
45. Weinstock PH, et al. Lipoprotein lipase controls fatty acid entry into adipose tissue, but fat mass is preserved by endogenous synthesis in mice deficient in adipose tissue lipoprotein lipase. *Proc Natl Acad Sci U S A.* 1997;94(19):10261-6.
46. Lafferty MJ, Bradford KC, Erie DA, and Neher SB. Angiopoietin-like protein 4 inhibition of lipoprotein lipase: evidence for reversible complex formation. *J Biol Chem.* 2013;288(40):28524-34.
47. Mysling S, et al. The angiopoietin-like protein ANGPTL4 catalyzes unfolding of the hydrolase domain in lipoprotein lipase and the endothelial membrane protein GPIHBP1 counteracts this unfolding. *Elife.* 2016;5:e20958
48. Collins S, Daniel KW, Rohlfs EM, Ramkumar V, Taylor IL, and Gettys TW. Impaired expression and functional activity of the beta 3- and beta 1-adrenergic receptors in adipose tissue of congenitally obese (C57BL/6J ob/ob) mice. *Mol Endocrinol.* 1994;8(4):518-27.
49. McQueen AE, et al. The C-terminal fibrinogen-like domain of angiopoietin-like 4 stimulates adipose tissue lipolysis and promotes energy expenditure. *J Biol Chem.* 2017;292(39):16122-34.
50. Valenzuela DM, et al. High-throughput engineering of the mouse genome coupled with high-resolution expression analysis. *Nat Biotechnol.* 2003;21(6):652-9.
51. Folch J, Lees M, and Sloane Stanley GH. A simple method for the isolation and purification of total lipides from animal tissues. *J Biol Chem.* 1957;226(1):497-509.
52. Quehenberger O, Armando AM, and Dennis EA. High sensitivity quantitative lipidomics analysis of fatty acids in biological samples by gas chromatography-mass spectrometry. *Biochim Biophys Acta.* 2011;1811(11):648-56.
53. Green H, and Kehinde O. An established preadipose cell line and its differentiation in culture. II. Factors affecting the adipose conversion. *Cell.* 1975;5(1):19-27.
54. Yin W, et al. Genetic variation in ANGPTL4 provides insights into protein processing and function. *J Biol Chem.* 2009;284(19):13213-22.

Fig. 1

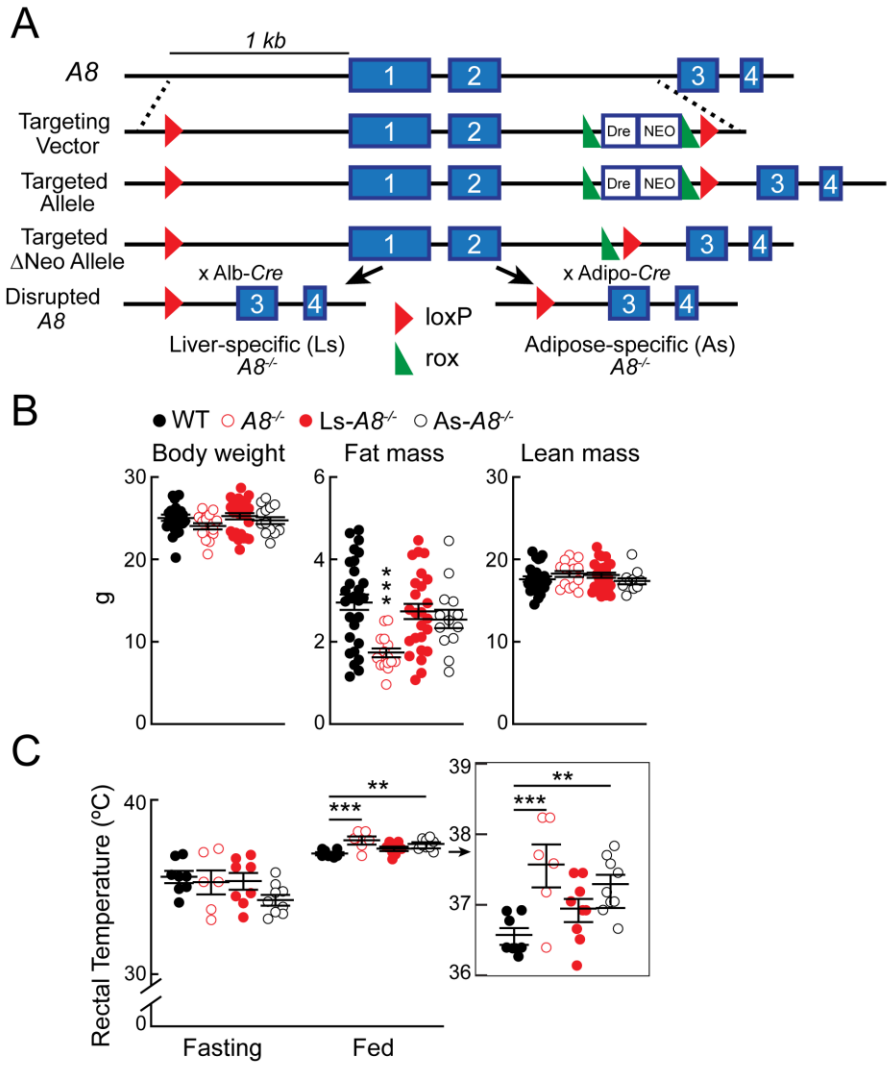

Figure 1

Tissue-specific disruption of *A8* in hepatocytes and adipocytes (A) and the body weights (B) and rectal temperatures (C) of mice. Schematic of mouse *A8*, the targeting vector, the targeted allele, the targeted ΔNeo allele, and the disrupted *A8* allele. LoxP sites were placed upstream of exons 1 and in intron 2. A rox-Dre-NEO-rox-loxP cassette was inserted in intron 2. After selection for Neo, *Dre* recombinase was expressed to excise the Neo cassette. Mice with the targeted ΔNeo allele (*fl/fl*) were crossed with mice expressing *Cre* under the control of the

albumin or adiponectin promoter to inactivate *A8* in hepatocytes [Liver-specific (Ls) $A8^{-/-}$ mice] or in adipocytes [Adipose-specific (As) $A8^{-/-}$ mice]. (B) Mean (± SEM) body weight were determined and then fat mass and lean body mass of chow-fed male mice (n=13-28/genotype, 9-10 wk) were measured using nuclear magnetic resonance. (C) Male mice (n=6-9/genotype, 9-10 wk) were maintained at room temperature (21–23°C). Rectal temperatures were obtained at the end of a 15 h fast (left) and then 4 h after chow was provided to the mice (right). The experiments were repeated three times and the results were similar. Values are means ± SEM. Groups were compared using one-way ANOVA with Dunnett`s multiple comparison test. **P < 0.01, ***P <0.001.

Fig. 2

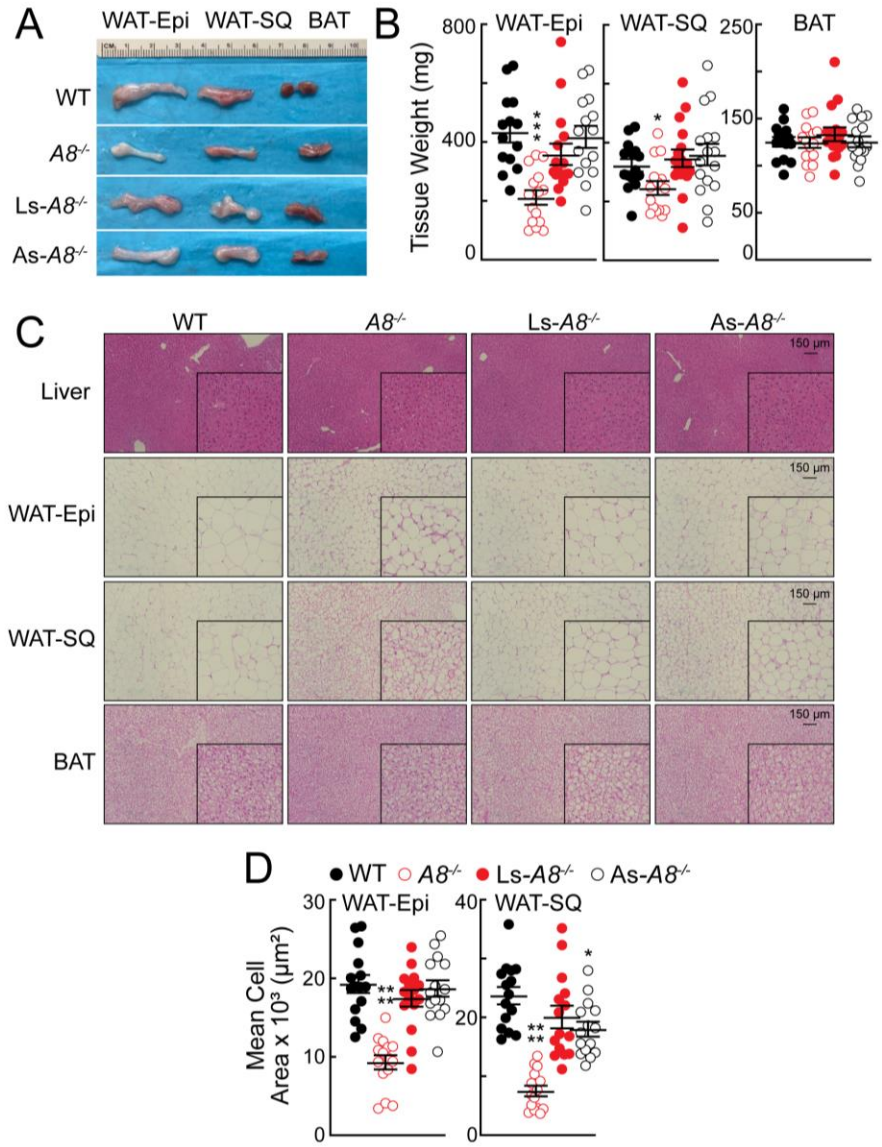

Figure 2

Adipose tissue morphology in chow-fed mice of the indicated genotypes. (A) Representative images of WAT and BAT fat pads in age-matched male mice (6/genotype, 11-12 wk). (B) Mean tissue weights (± SEM) of fat pads from age-matched male mice (n=4/5/genotype, 9-14 wk). Data were pooled from 3 independent experiments (n=14-

16/genotype). Values were compared using Two-way ANOVA. (C) Representative H&E staining of tissue sections (n=6/genotype; 12-13 wk). Magnification: 20X; Scale bars: 1 mm=150 μm) (D) Adipocyte size was quantified using ImageJ (NIH): 3 fields/tissue section. Values are means (± SEM) from 3 fields. Groups were compared using one-way ANOVA with Dunnett`s multiple comparison test. *P < 0.05; ***P < 0.001; ****P<0.0001. WAT, white adipose tissue. Epi, WAT-epididymal; SQ, subcutaneous; BAT, brown adipose tissue.

Fig. 3

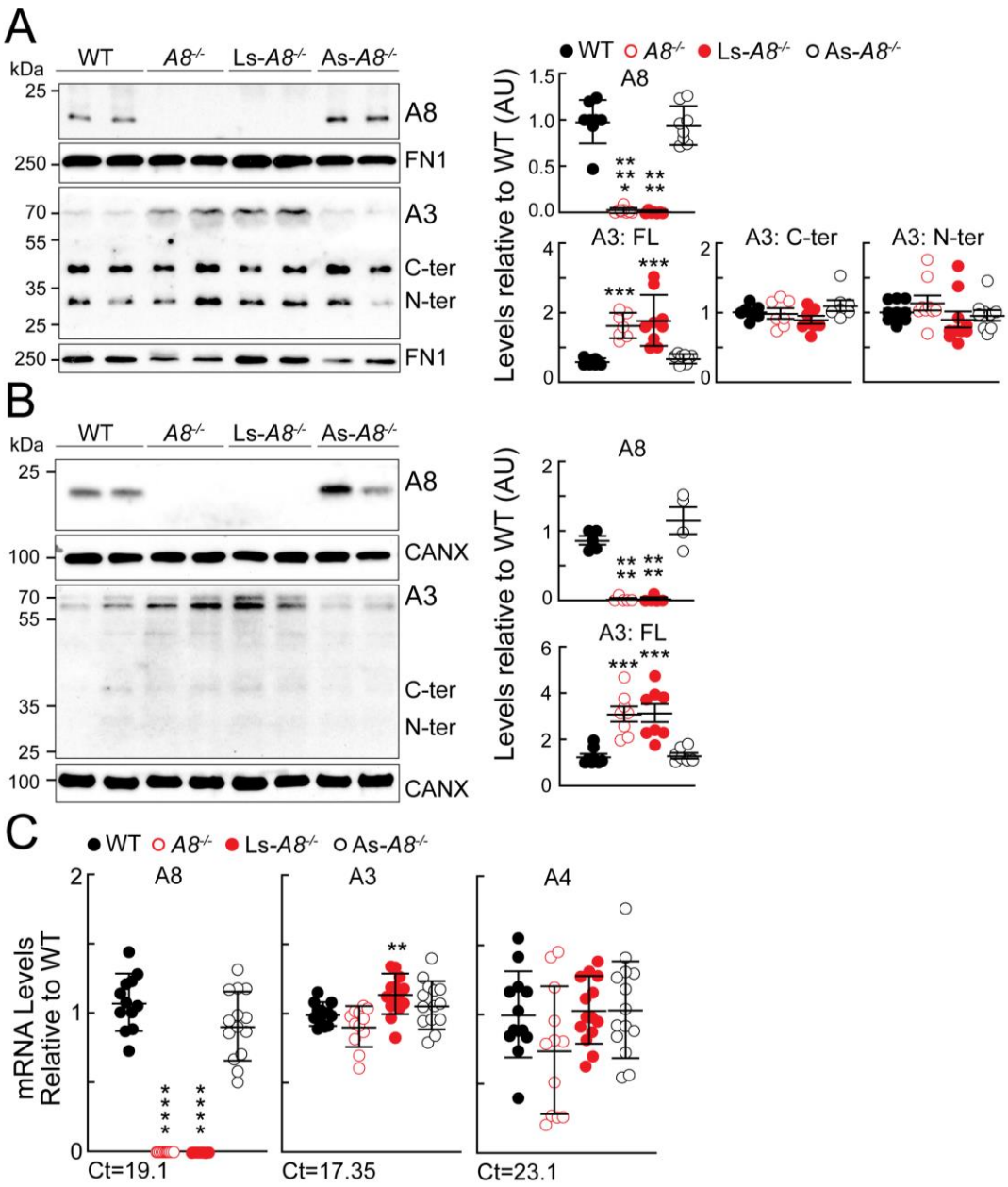

Figure 3

Immunoblot analysis of A3 and A8 in plasma (A) and liver lysates (B) in mice of the indicated genotypes. Age-matched, chow-fed male mice (n=7-8/genotype, 9-12 wk) were

subjected to a 3-day fasting and refeeding protocol, as described in the Methods. All experiments were performed in refed conditions. Immunoblot analysis of (A) plasma samples (1.5 μl) and (B) liver lysates (50 μg) was performed using anti-A8, anti-A3, and anti-fibronectin (FN1) or anti-calnexin (CANX) antibodies as described in the Methods. The intensity of the bands was determined by LI-COR Image Studio™ Lite. Data were pooled from two experiments (n=3-4/group/experiment). Values represent means (± SEM). Groups were compared using two-way ANOVA. (C) Messenger RNA levels of hepatic A3, A4 and A8 were determined by Real-time PCR on 3 independent groups of animals (n=4-5/genotype) and the results were pooled and expressed relative to WT mice as described in the Methods. Cycle threshold (Ct) values in the WT mice are provided. Groups were compared using two-way ANOVA. **P <0.01, ***P <0.001, ****P <0.0001, *****P <0.00001.

Fig. 4

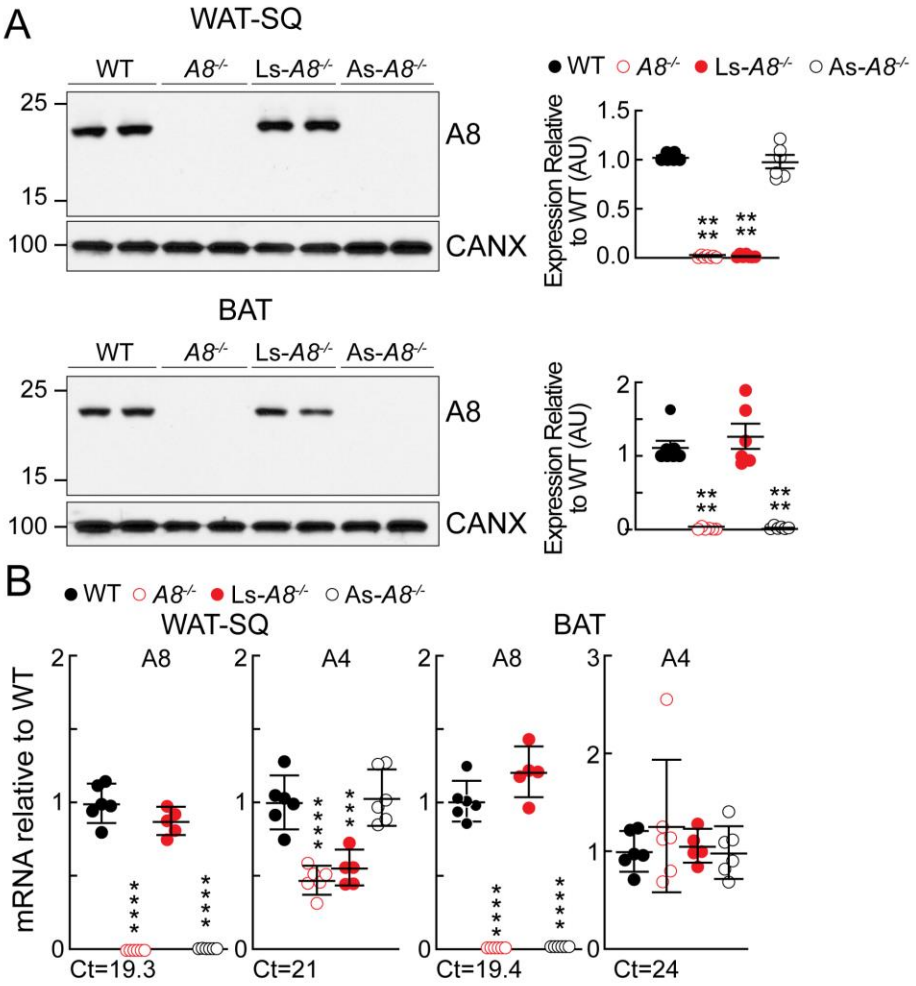

Figure 4

A8 protein (A) and mRNA levels (B) in WAT and BAT of mice of the indicated genotypes.

(A) Immunoblot analysis of A8 in tissue lysates from WAT-SQ and BAT (25 µg each) of chow-fed male mice (n=3-4/genotype, 12-13 wk) was performed as described in the Methods. All experiments were performed in refed conditions. Pooled data from two experiments (n=3-4/group for each experiment) is shown. Band intensities were normalized to the level of calnexin (CANX) and then expressed relative to WT. (B) Messenger RNA t levels of A8 and A4 were determined by Real-time PCR in chow-fed male mice (n=6/group, 12-13 wk). Values are

expressed as ratios compared with the mean level in WT littermates, which was set at 1. Cycle threshold (Ct) values in the WT mice are provided. ***P <0.001, ****P <0.0001. Groups were compared using two-way ANOVA. The experiments were repeated twice and the results were similar.

Fig. 5

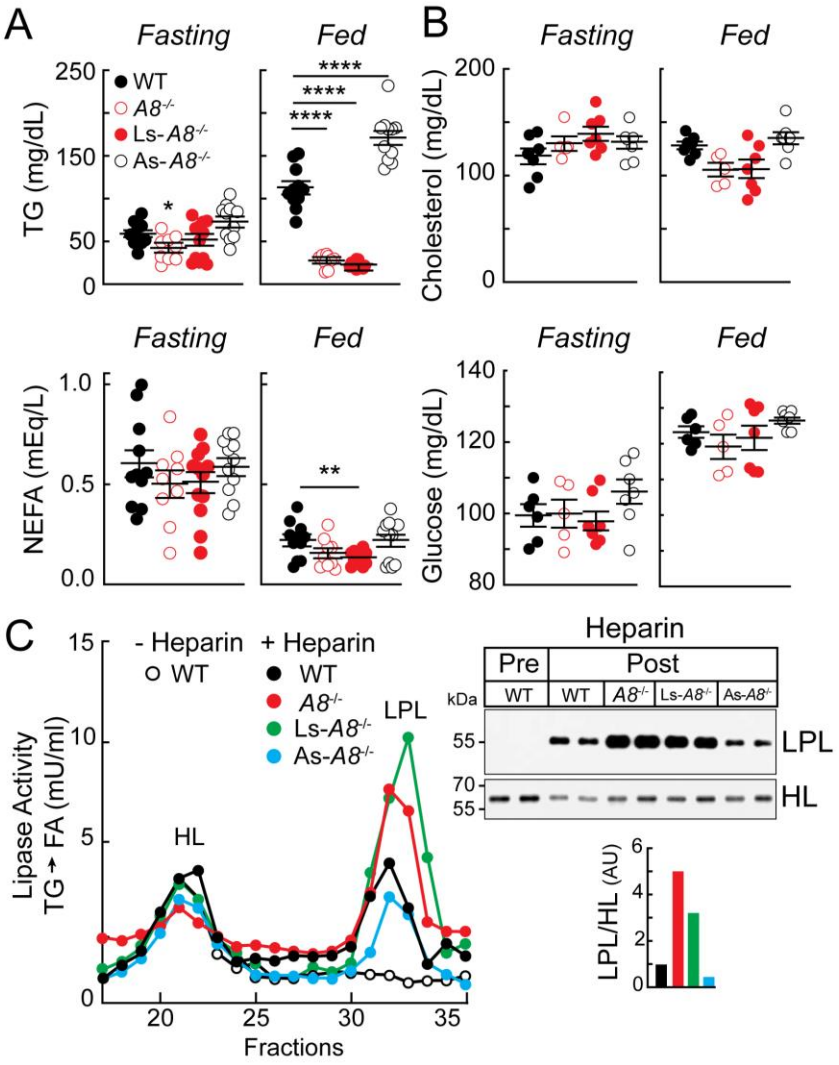

Figure 5

Plasma lipid and glucose levels (A, B), post-heparin plasma lipase activities and intravascular lipoprotein lipase (LPL) levels (C) in mice of the indicated genotypes. (A) Diets of age-matched male mice (n = 5~6/group, 10-15 wk) were synchronized as described in the Methods. Plasma samples were obtained at the end of the last fasting period (*Fasting*) and then 4 h after refeeding (*Fed*) and levels of TG, nonesterified fatty acids (NEFA) (B) cholesterol, were measured in duplicate (5 μl). Plasma glucose levels were measured from the first drop of blood from the tail vein. Values are means (± SEM). The experiment was repeated and the data was similar. Groups were compared using two-way ANOVA. *P < 0.05, **P <0.01, ****P <0.0001. The experiment was performed 3 times and the compiled results are shown. (C) The diets of the mice were handled as described in panel A. Four hours after refeeding, blood was collected from the WT mice. Mice were then injected with heparin intravenously (1 U/g) and blood was collected after 15 min. Pooled plasma was fractionated on a heparin column (1 ml) to separate hepatic lipase (HL) and LPL. TG lipase activity was measured from 50 μl from each fractions as described in Methods. Pooled plasma samples (10 μl) were diluted to 500 μl with PBS and incubated with heparin beads (20 μl) for 2 h. The heparin beads-bound proteins were subjected to immunoblotting using anti-mouse LPL and HL polyclonal Abs, as described in the Methods. Quantitative values are expressed as ratios to the level of HL and expressed relative to the WT value, which was set to 1.

Fig. 6

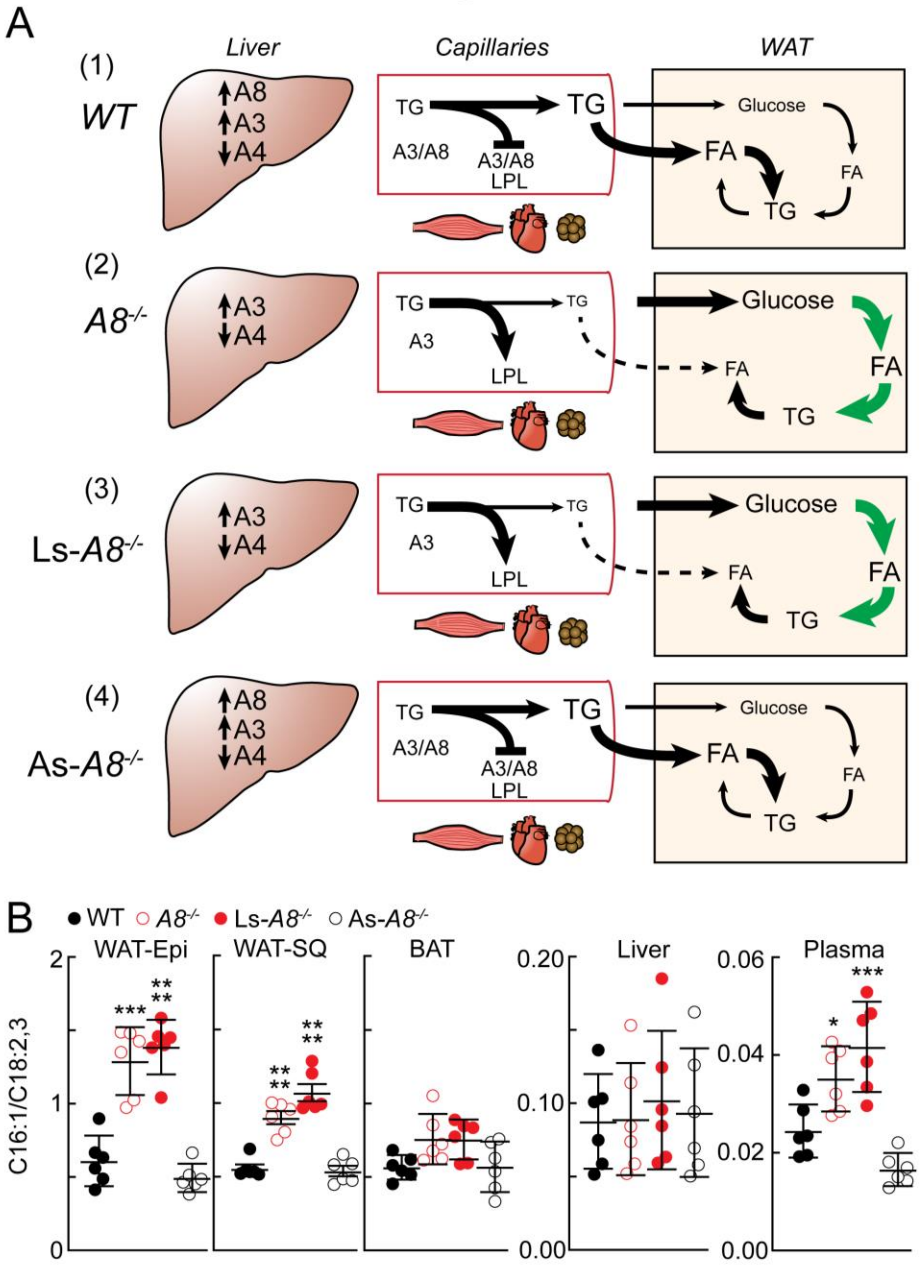

Figure 6

A schematic showing the role of hepatic A8 and A3 in triglyceride (TG) trafficking in the fed state. (A) Expression of both A8 and A3 mRNA increase and A4 mRNA levels decrease with feeding (11). (1) A3 and A8 form a complex that inactivates intravascular LPL, which is

most active in oxidative tissues. As a result, circulating TG is available for hydrolysis and uptake by adipose tissue. (2) Absence of A8 results in more TGs being available for uptake by oxidative tissues, and less being available for uptake by adipose tissue. Glucose uptake, and its conversion to TG, is enhanced in adipose tissue of *A8*$^{-/-}$ mice. (3) TG trafficking in the Ls-*A8*$^{-/-}$ mice resembles that of the *A8*$^{-/-}$ mice (4) whereas TG trafficking in the As-*A8*$^{-/-}$ mice resembles that seen in the WT animals. (B) Levels of C16:1 (endogenously synthesized) and C18:2 and C18:3 (diet-derived) in plasma and tissue lysates (adipose tissue and liver) were measured as described in the Methods and the mean ratio (± SEM) of C16:1 to C18:2 plus C18:3 in each tissue is shown. Groups were compared using one-way ANOVA with Dunnett`s multiple comparison test. *P < 0.05, ***P <0.001, ****P <0.0001.

Fig. 7

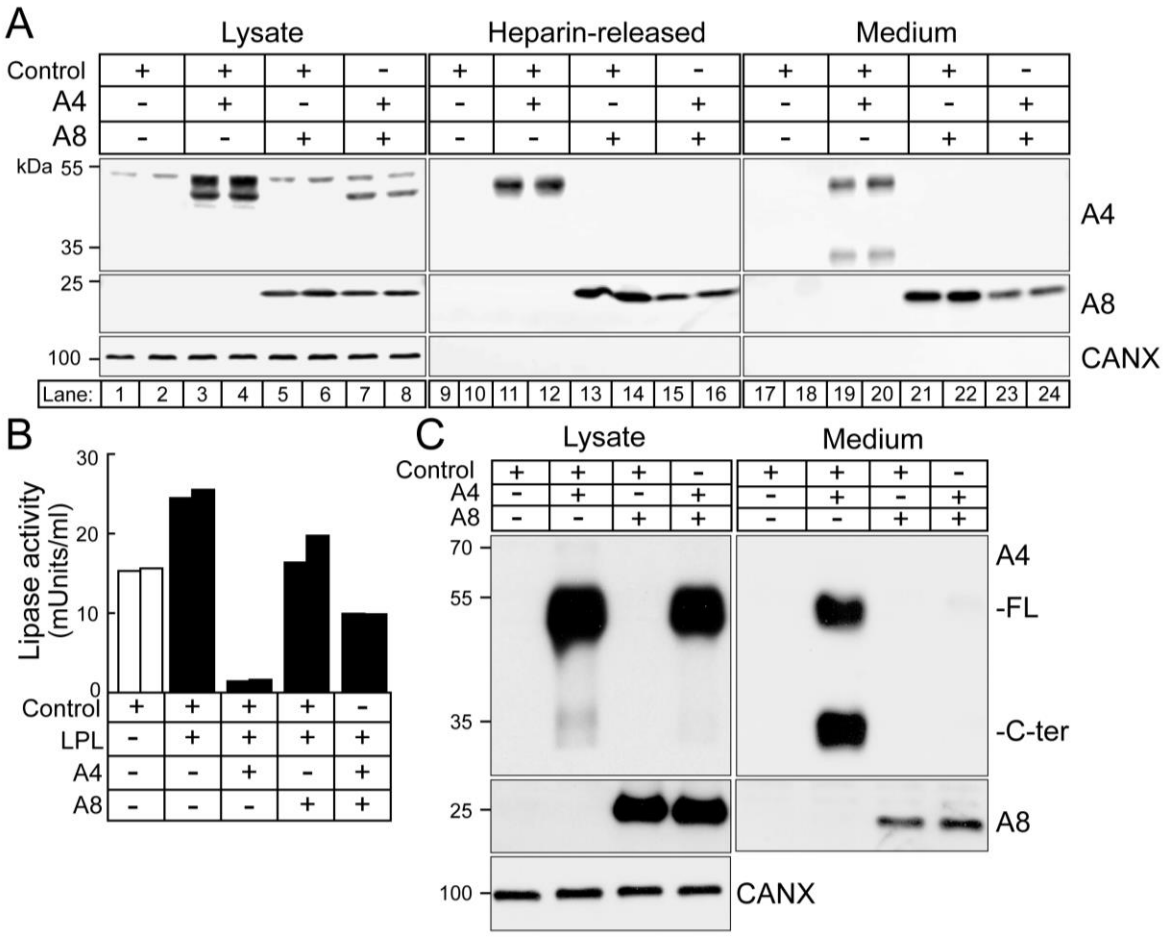

Figure 7

A8 prevents A4 secretion (A) and attenuates A4 inhibition on LPL (B) in CHO-K1 cells and (C) in 3T3 adipocytes. (A) Equimolar amounts of control (empty plasmid), recombinant A4 and A8 were expressed in CHO-K1 cells alone or together. Whole cell lysates, the heparin-released fraction, and conditioned medium were subjected to SDS-PAGE and immunoblotting using anti-A4 (top), anti-A8 (middle) and anti-calnexin (CANX) Abs as described in the Methods. (B). CHO-K1 cells were co-transfected with control, A4, A8, and LPL plasmids as indicated. The LPL activity was assayed in the medium 48 h after transfection, as described in the Methods. (C) Differentiated 3T3-L1 adipocytes were infected with control and single or combination of A8 and

A4 adenoviruses as described in the Methods. After 24 h, cells and medium were collected and immunoblot analysis was performed using anti-A4 (top), anti-A8 (middle) and anti-calnexin (CANX) Abs on cell lysates and cultured medium. The experiments were performed two additional times and the results were similar.

Fig. 8

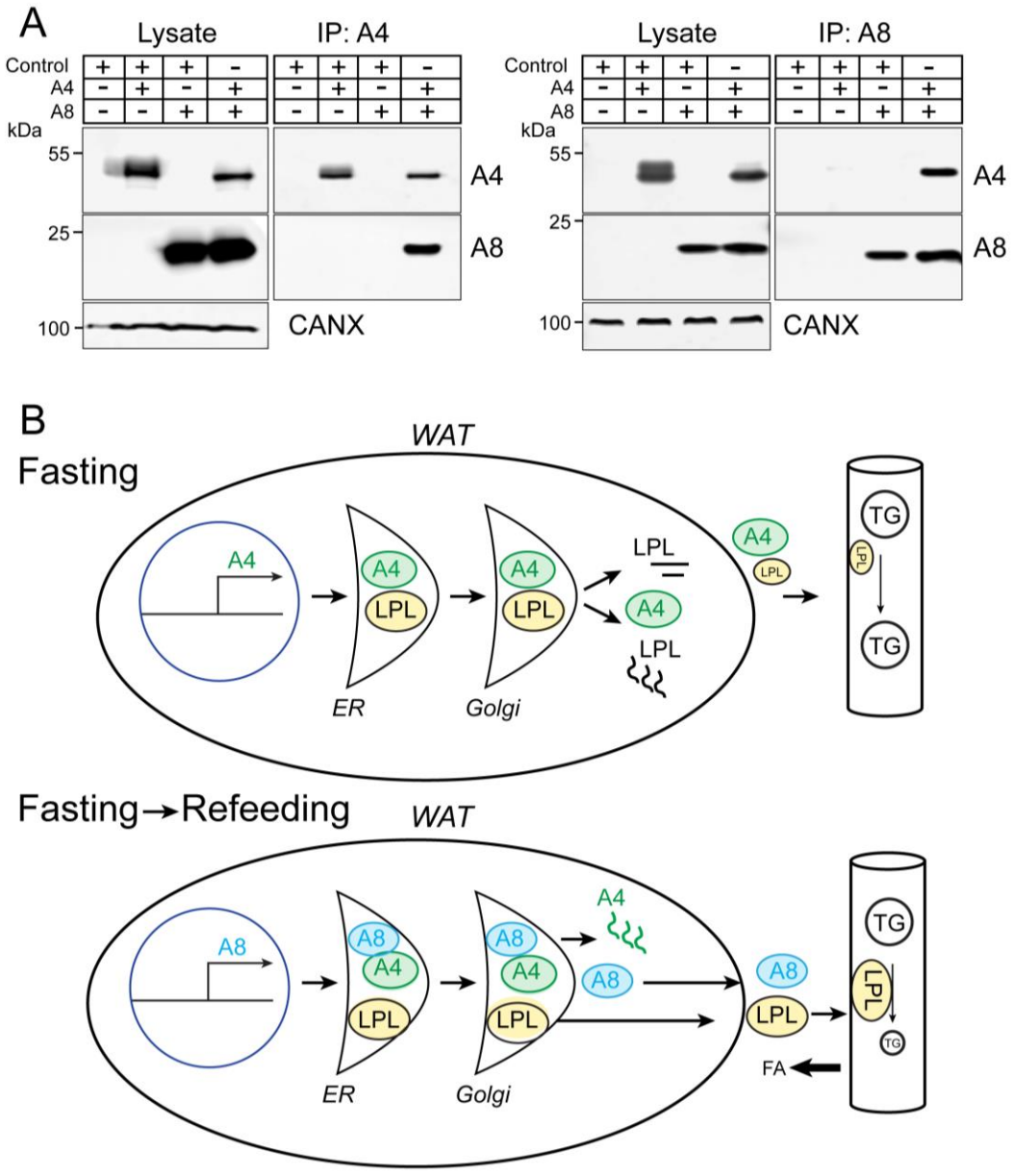

Figure 8

A8 inhibits A4-mediated LPL degradation by interacting with A4. (A) A8 physically interacts with A4 in QBI-293 cells. Recombinant A4-myc and A8-Flag were co-expressed in QBI-293 cells alone (with empty plasmid) or together. A4 was immunoprecipitated using Myc-linked magnetic beads (left panel) and A8 was immunoprecipitation using Flag-magnetic beads (right panel) as described in the Methods. As A4 has non-specific binding to magnetic beads, Flag-beads were eluted using 3X Flag peptide. Immunoblot analysis using anti-A4 (top), anti-A8 (middle) and anti-calnexin (CANX) Abs was performed using 30 μg of lysate (input) as described in Methods. (B) Schematic model of A4, A8 and LPL expression in WAT from fasted (top) and refed (bottom) mice. After a 15 h fast, no A8 is present in the adipose tissue of WT mice whereas levels of expression of A4 are high. A4 expression promotes degradation of LPL. As a consequence, circulating lipoproteins bypass WAT and deliver TG to oxidative tissues (Top). In the fasting to feeding transition, A8 expression rises as levels of A4 slowly fall. A8 interacts with A4, thus sparing LPL from A4-stimulated intracellular degradation. LPL is now available to hydrolyze circulating lipoprotein-TG and thus replete TG stores in adipose tissue when food is available.

Supplementary Tables

Table S1. Offspring of matings of different genotypes

A. +/+ × Adipo-*Cre*Tg/+								
	Males n=309 (51%)				Females n=298 (49%)			
	Observed		Expected		Observed		Expected	
Genotype	No.	%	No.	%	No.	%	No.	%
+/+	167	54%	154	50	146	49%	149	50
Tg/+	142	46%	155	50	152	51%	149	50
B. +/+ × Alb-*Cre*Tg/+								
	Males n=50 (52%)				Females n= 46 (48%)			
	Observed		Expected		Observed		Expected	
Genotype	No.	%	No.	%	No.	%	No.	%
+/+	25	50%	25	50	19	41%	23	50
Tg/+	25	50%	25	50	27	59%	23	50
C. f/+ × f/+								
	Males n=105 (47%)				Females N=119 (53%)			
	Observed		Expected		Observed		Expected	
Genotype	No.	%	No.	%	No.	%	No.	%
+/+	35	33%	24	25	33	26%	21	25
f/+	42	40%	57	50	59	48%	77	50
f/f	28	27%	24	25	27	26%	21	25
D. f/f; +/+ x f/f; Adipo-*Cre*Tg/+								
	Males n= 230 (50%)				Females n= 229 (50%)			
	Observed		Expected		Observed		Expected	
Genotype	No.	%	No.	%	No.	%	No.	%
(f/f)(+/+)	123	53%	115	50	108	47%	115	50
(f/f)(Tg/+)	107	47%	115	50	121	53%	114	50
E. f/f; +/+ x f/f; Alb-*Cre*Tg/+								
	Males n=191 (59%)				Females n= 134 (41%)			
	Observed		Expected		Observed		Expected	
Genotype	No.	%	No.	%	No.	%	No.	%
(f/f)(+/+)	91	48%	95	50	83	62%	67	50
(f/f)(Tg/+)	100	52%	96	50	51	38%	67	50

Table S2. Litter size of different genotypes

A. +/+ × Adipo-CreTg/+					
Breedings			Pups		
Male	Female	No. of litters	Pups per litter	Males	Females
+/+	Tg/+	45	4.8	108	108
Tg/+	+/+	85	4.9	216	201
B. +/+ × Alb-CreTg/+					
Breedings			Pups		
Male	Female	No. of litters	Pups per litter	Males	Females
+/+	Tg/+	7	5.6	21	18
Tg/+	+/+	11	7.54	41	42
C. f/+ × f/+					
Breedings			Pups		
Male	Female	No. of litters	Pups per litter	Males	Females
(f/f)	(f/f)	5	7.2	19	17
(f/+)	(f/+)	56	4.5	118	132
(+/+)	(+/+)	1	4.0	3	1
D. f/f; +/+ x f/f; Adipo-CreTg/+					
Breedings			Pups		
Male	Female	No. of litters	Pups per litter	Males	Females
(f/f)(+/+)	(f/f)(Tg/+)	62	4.7	140	154
(f/f)(Tg/+)	(f/f)(+/+)	34	3.9	60	73
E. f/f; +/+ x f/f; Alb-CreTg/+					
Breedings			Pups		
Male	Female	No. of litters	Pups per litter	Males	Females
(f/f)(+/+)	(f/f)(Tg/+)	38	4.0	93	57
(f/f)(Tg/+)	(f/f)(+/+)	32	5.5	93	83

Table S3. Oligonucleotides used for RT-PCR

Gene	Forward primer, 5′-3′	Reverse primer, 5′-3′
36B4	CACTGGTCTAGGACCCGAGAAG	GGTGCCTCTGGAGATTTTCG
ACC	TGGACAGACTGATCGCAGAGAAAG	TGGAGAGCCCCACACACA
ACL	GCCAGCGGGAGCACATC	CTTTGCAGGTGCCACTTCATC
ACS	GCTGCCGACGGGATCAG	TCCAGACACATTGAGCATGTCAT
ADIPOQ	AGATGGCACTCCTGGAGAGAA	TTCTCCAGGCTCTCCTTTCCT
ADRB2	GGTTATCGTCCTGGCCATCGTGTTTG	TGGTTCGTGAAGAAGTCACAGCAAGTCTC
ADRB3	TCTAGTTCCCAGCGGAGTTTTCATCG	CGCGCACCTTCATAGCCATCAAACC
AGPAT1	GCTGGCTGGCAGGAATCAT	GTCTGAGCCACCTCGGACAT
AGPAT2	TTTGAGGTCAGCGGACAGAA	AGGATGCTCTGGTGATTAGAGATGA
AGPAT3	CCAGTGGCTTCACAAGCTGTAC	CCCTGGGAATACACCCTTCTG
ANGPTL3	AGCAAGACAACAGCATAAGAGAACTC	TGAGCTGCTTTTCTATTTCTTTTATCTG
ANGPTL4	GCCTTTCCCTGCCCTTCTC	GATTGGAATGGCTACAGGTACCA
ANGPTL8	ACATGGCTGTGCTTGCTCTCT	CAAATTCTTGGTGGGCTTGAC
ATGL	GAGAGAACGTCATCATATCCCACTT	CCACAGTACACCGGGATAAATGT
CD36	GGAACTGTGGGCTCATTGC	CATGAGAATGCCTCCAAACAC
CHREBPα	CGACACTCACCCACCTCTTC	TTGTTCAGCCGGATCTTGTC
CHREBPβ	TCTGCAGATCGCGTGGAG	CTTGTCCCGGCATAGCAAC
CIDEA	CCGAGTACTGGGCGATACAGA	GGTTACATGAACCAGCCTTTGG
CPT1A	CACCAACGGGCTCATCTTCTA	CAAAATGACCTAGCCTTCTATCGAA
CPT2	AGCCTACCTGGTCAATGCATATC	GGGTTTGGGTATACGAGTTGAATT
CYCLO	TGGAGAGCACCAAGACAGACA	TGCCGGAGTCGACAATGAT
DIO2	CATTGATGAGGCTCACCCTTC	GGTTCCGGTGCTTCTTAACCT
ELOVL6	TGTACGCTGCCTTTATCTTTGG	GCGGCTTCCGAAGTTCAA
Eva1	CCACTTCTCCTGAGTTTACAGC	GCATTTTAACCGAACATCTGTCC
FABP4	ACTGGGCGTGGAATTCGATGA	ACCAGCTTGTCACCATCTCGT
FABP5	CGGGTCTATGAGAAGGTGCAA	GAGCATATTCACTCTGGCAGCTAA
FAS	GCTGCGGAAACTTCAGGAAAT	AGAGACGTGTCACTCCTGGACTT
GLUT4	CCGGCAGCCTCTGATCAT	CCGACTCGAAGATGCTGGTT
G6P	TGGGCAAAATGGCAAGGA	TCTGCCCCAGGAATCAAAAAT
HK2	TGCCAAGCGTCTCCATAAGG	GGAGGAAGCGGACATCACAA
HMGCR	CTTGTGGAATGCCTTGTGATTG	AGCCGAAGCAGCACATGAT
HPRT	CCTCATGGACTGATTATGGACAG	AATCCAGCAGGTCAGCAAAG
HSL	GGAGCACTACAAACGCAACGA	TCGGCCACCGGTAAAGAG
LPL	ACTCTGTGTCTAACTGCCACTTCAA	ATACATTCCCGTTACCGTCCAT
LXRA	TCTGGAGACGTCACGGAGGTA	CCCGGTTGTAACTGAAGTCCTT
PGC1α	AACCACACCCACAGGATCAGA	TCTTCGCTTTATTGCTCCATGA
PPARα	ACAAGGCCTCAGGGTACCA	GCCGAAAGAAGCCCTTACAG
PPARγ	CACAATGCCATCAGGTTTGG	GCTGGTCGATATCACTGGAGATC
PPARγ2	TGCCTATGAGCACTTCACAAGAAAT	CGAAGTTGGTGGGCCAGAA
PPARδ	ACGCACCCTTTGTCATCCA	TTCCACACCAGGCCCTTCT
PRDM16	CCCCACATTCCGCTGTGAT	CTCGCAATCCTTGCACTCA

RGS16	GGGCTCACCACATCTTTGAC	TTGGTCAGTTCTCGGGTCTC
SCD1	CCGGAGACCCCTTAGATCGA	TAGCCTGTAAAAGATTTCTGCAAACC
SREBP-1c	GGAGCCATGGATTGCACATT	GGCCCGGGAAGTCACTGT
SREBP-2	GCGTTCTGGAGACCATGGA	ACAAAGTTGCTCTGAAAACAAATCA
TXNIP	TATGTACGCCCCTGAGTTCCA	GTTAAGGACGCACGGATCCA
UCP1	ACTGCCACACCTCCAGTCATT	CTTTGCCTCACTCAGGATTGG

Supplementary Figures

Fig. S1

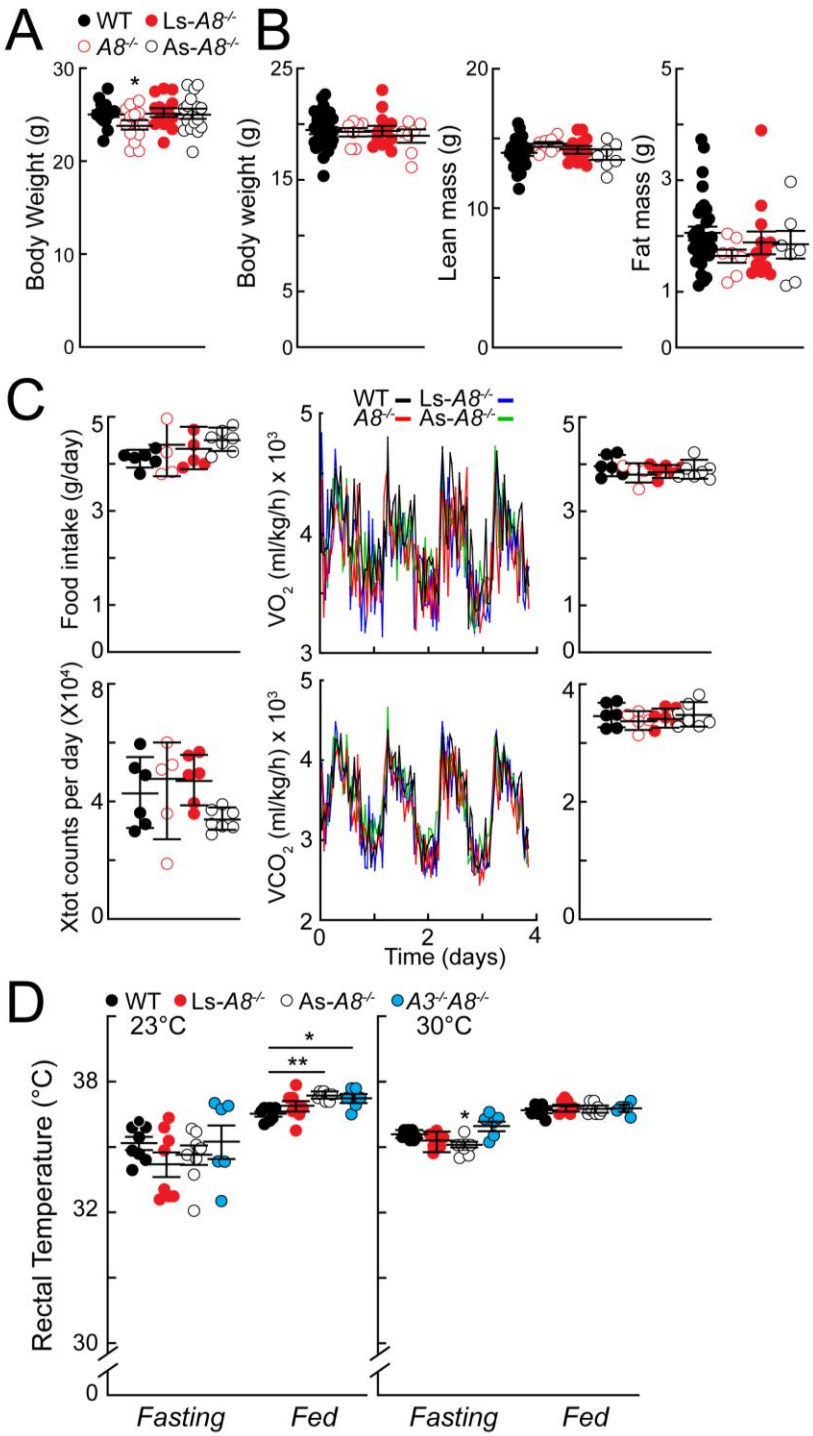

Figure S1

Body weights (A), indirect calorimetry (B) and rectal temperatures (C) of WT(fl/fl), *A8*$^{-/-}$, Ls-*A8*$^{-/-}$, and As-*A8*$^{-/-}$ male mice. (A) Body weights (± SEM) were obtained from age-matched male mice (n=4-5/genotype, 9-14 wk). Data shown were pooled from 3 independent experiments (14/genotype) and compared using two-way ANOVA. (B) Body weights (± SEM) of age-matched female mice (n=7-32/genotype, 9-10 wk). (C) Age-matched male mice (n=5–7/genotype, 11-16 wk) were housed individually in metabolic cages for seven days. Food intake and activity were monitored (right). Both O_2 consumption and CO_2 output were measured for 2 min at 50-min intervals for 4 consecutive days (right). Group means ± SEM for VO_2 consumption and VCO_2 output are provided (right panels). (D) Age-matched male Mice (n=6-8 per group, 12-15 wk) were housed individually in metabolic cages at 30°C for 3 weeks. Rectal temperatures were obtained at the end of a 15 h fast (left) and then 4 h after chow was provided (right). Groups were compared using one-way ANOVA with Dunnett`s multiple comparison test. * $P<0.05$, ** $P<0.01$.

Fig. S2

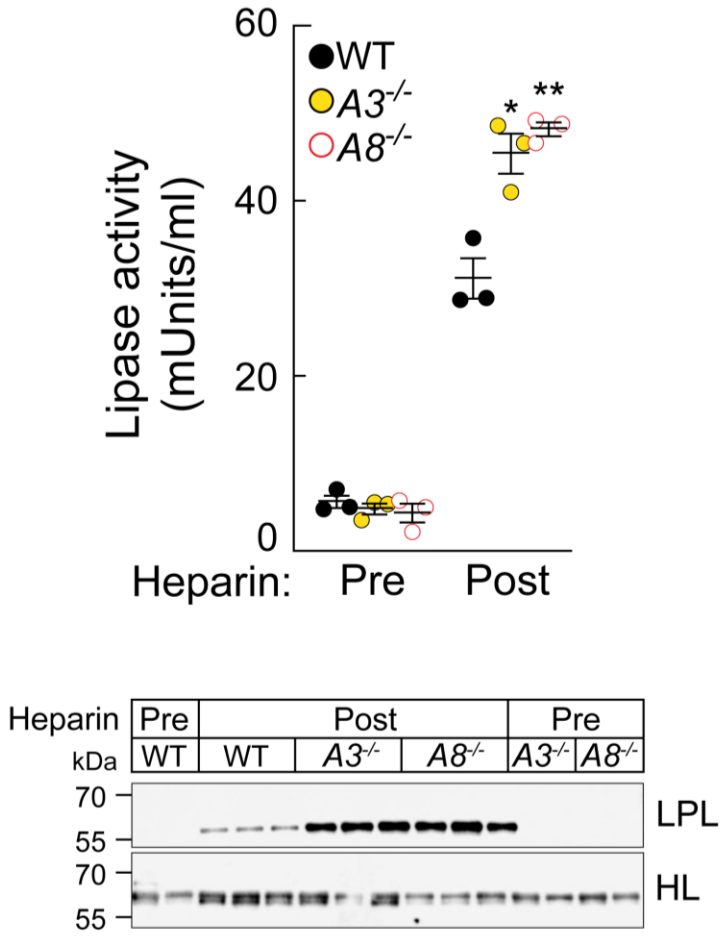

Figure S2

Intravascular LPL activity and mass are similar in *A3*$^{-/-}$ and *A8*$^{-/-}$ mice. The diets of the male mice (n=3/genotype, 13-16 wk) were synchronized for 3 days as described in the Methods. Four hours after refeeding, blood was obtained from WT mice and the mice were injected with heparin intravenously (1 U/g). Blood was collected after 15 min and lipase activity was measured as described in the legend to Figure 5 (Top). A total of 10 μl of plasma from each mouse was diluted to 500 μl in PBS and incubated with 20 μl of heparin beads for 2 h. The

heparin-bound proteins were subjected to immunoblotting for LPL and hepatic lipase (HL). Groups were compared using one-way ANOVA with Dunnett`s multiple comparison test. *P<0.05, **P <0.01.

Fig. S3

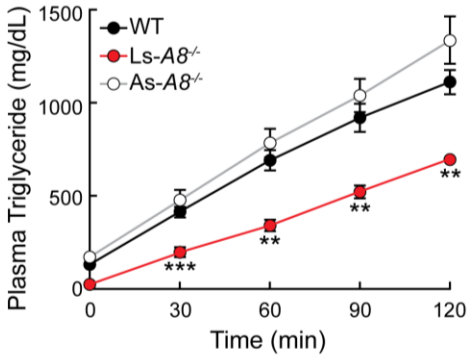

Figure S3.

VLDL-TG secretion rates in WT, Ls-*A8*$^{-/-}$ and As-*A8*$^{-/-}$mice. The diets of female mice (n=4/genotype, 7-9 wk) were synchronized for 3 days as described in the Methods. At the end of the fasting cycle on day 3, mice were given access to food for 4 hours and then injected with a bolus of Triton WR-1339 (500 mg/kg) via the tail vein. Blood was collected from the tail vein at the indicated times, and TG levels were measured in plasma. The slopes of the lines were calculated assuming a linear increase in TG concentrations over time, and compared using unpaired two-tailed Student's *t* tests. **P<0.01, ***P<0.001.

Fig. S4

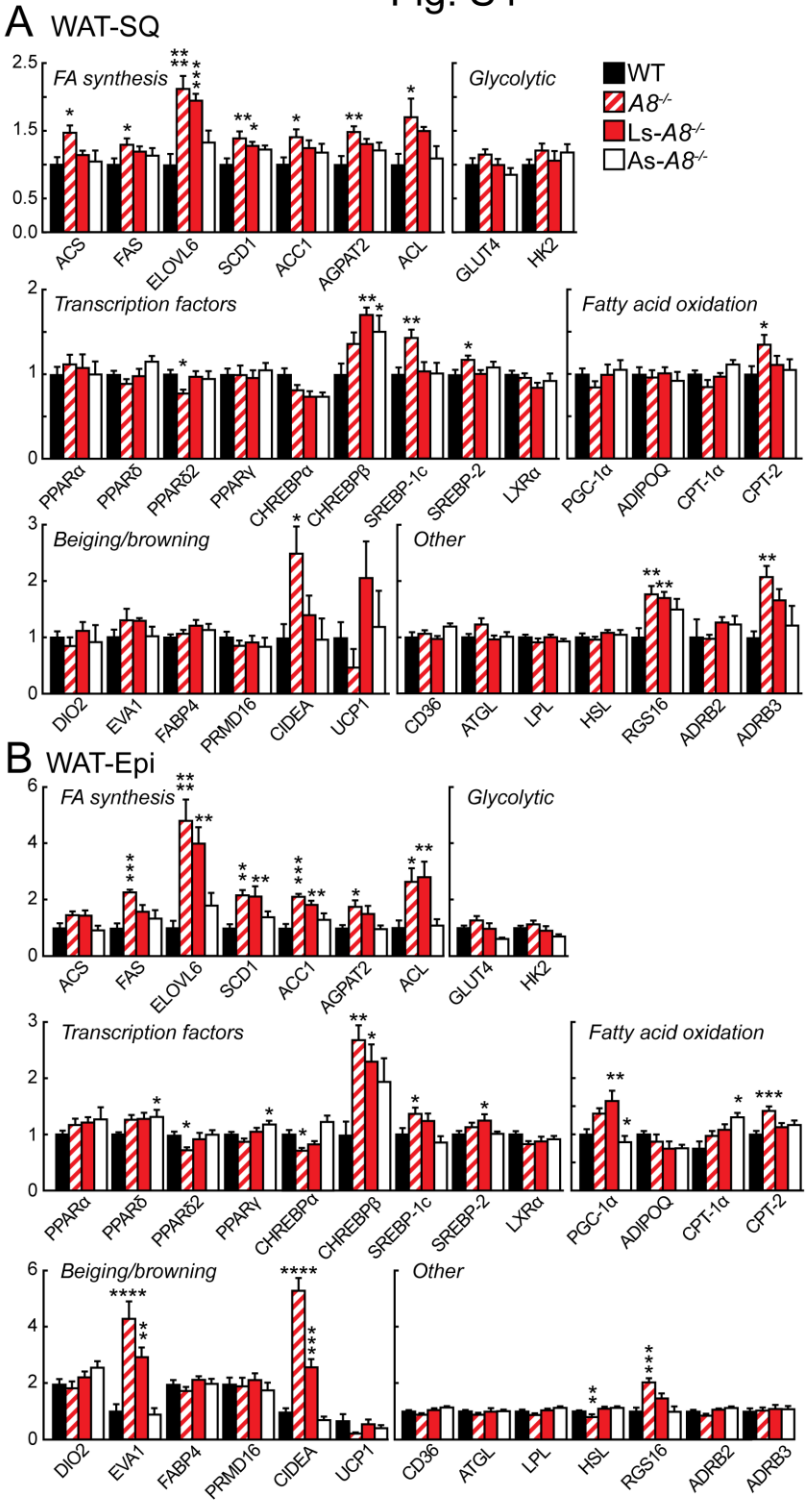
A WAT-SQ
FA synthesis
Glycolytic
WT
A8-/-
Ls-A8-/-
As-A8-/-
ACS
FAS
ELOVL6
SCD1
ACC1
AGPAT2
ACL
GLUT4
HK2
Transcription factors
Fatty acid oxidation
PPARα
PPARδ
PPARδ2
PPARγ
CHREBPα
CHREBPβ
SREBP-1c
SREBP-2
LXRα
PGC-1α
ADIPOQ
CPT-1α
CPT-2
Beiging/browning
Other
DIO2
EVA1
FABP4
PRMD16
CIDEA
UCP1
CD36
ATGL
LPL
HSL
RGS16
ADRB2
ADRB3
B WAT-Epi
FA synthesis
Glycolytic
Transcription factors
Fatty acid oxidation
Beiging/browning
Other

Fig. S4

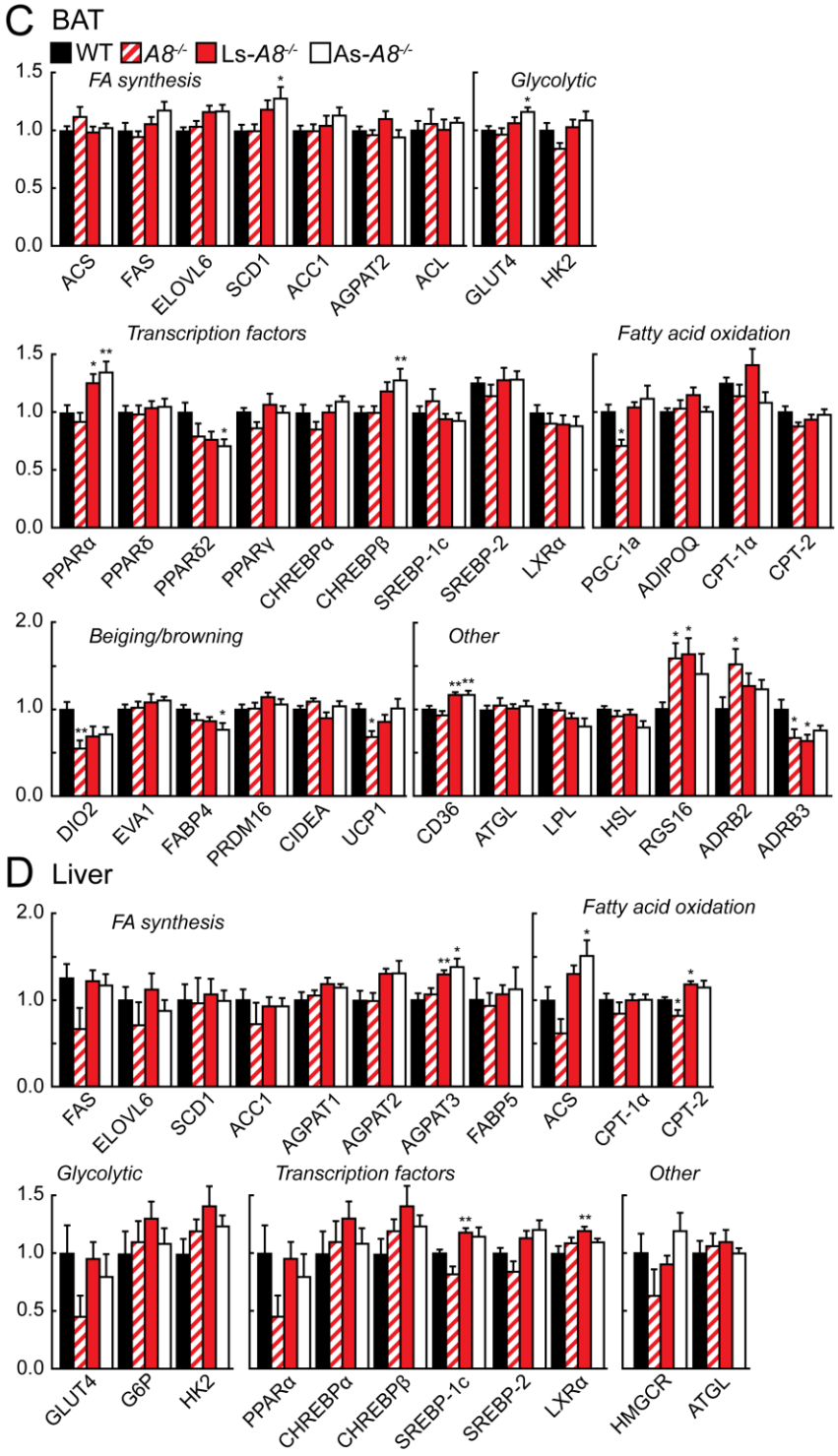
C BAT
WT A8-/- Ls-A8-/- As-A8-/-
FA synthesis
Glycolytic
ACS
FAS
ELOVL6
SCD1
ACC1
AGPAT2
ACL
GLUT4
HK2
Transcription factors
Fatty acid oxidation
PPARα
PPARδ
PPARδ2
PPARγ
CHREBPα
CHREBPβ
SREBP-1c
SREBP-2
LXRα
PGC-1a
ADIPOQ
CPT-1α
CPT-2
Beiging/browning
Other
DIO2
EVA1
FABP4
PRDM16
CIDEA
UCP1
CD36
ATGL
LPL
HSL
RGS16
ADRB2
ADRB3
D Liver
FA synthesis
Fatty acid oxidation
FAS
ELOVL6
SCD1
ACC1
AGPAT1
AGPAT2
AGPAT3
FABP5
ACS
CPT-1α
CPT-2
Glycolytic
Transcription factors
Other
GLUT4
G6P
HK2
PPARα
CHREBPα
CHREBPβ
SREBP-1c
SREBP-2
LXRα
HMGCR
ATGL

Figure S4.

Messenger RNA levels in adipose tissue and liver of male mice of the indicated genotypes. Male mice (n=6/genotype, 12-13 wk) were fasted overnight and then fed for 4 hours. Fold changes in levels of selected mRNAs encoding enzymes and transcription factors involved in fatty synthesis and oxidation, glycolysis, and thermogenesis/ browning are shown. Transcript levels were determined by Real-Time-PCR as described in the Methods. Data are expressed as means ± SEM. Groups were compared using one-way ANOVA with Dunnett`s multiple comparison test. *P < 0.05; **P < 0.01; ***P < 0.001, ****P < 0.0001. The experiment was repeated once, and the results were similar.

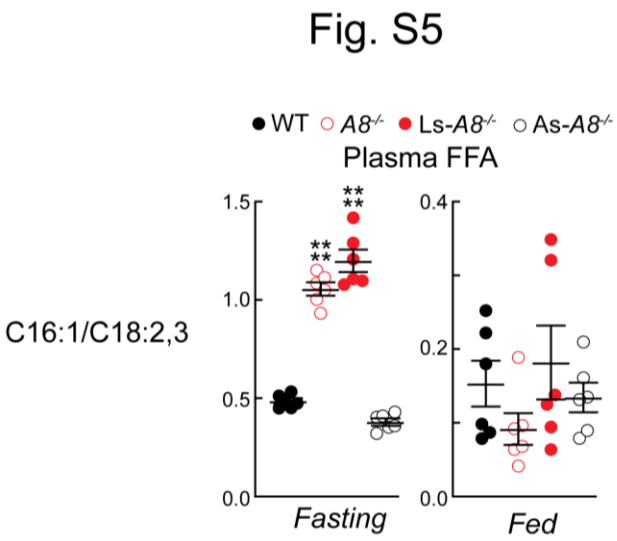

Figure S5.

C16:1 and C18:2,3 levels in circulating free fatty acids.

Levels of C16:1 (endogenously synthesized) and C18:2 and C18:3 (diet-derived) were measured in fasting and fed plasma free fatty acid pool as described in the Methods and the mean ratios (± SEM) of C16:1 to C18:2 plus C18:3 is shown. Groups were compared using one-way ANOVA with Dunnett`s multiple comparison test. ****P <0.0001.

Fig. S6

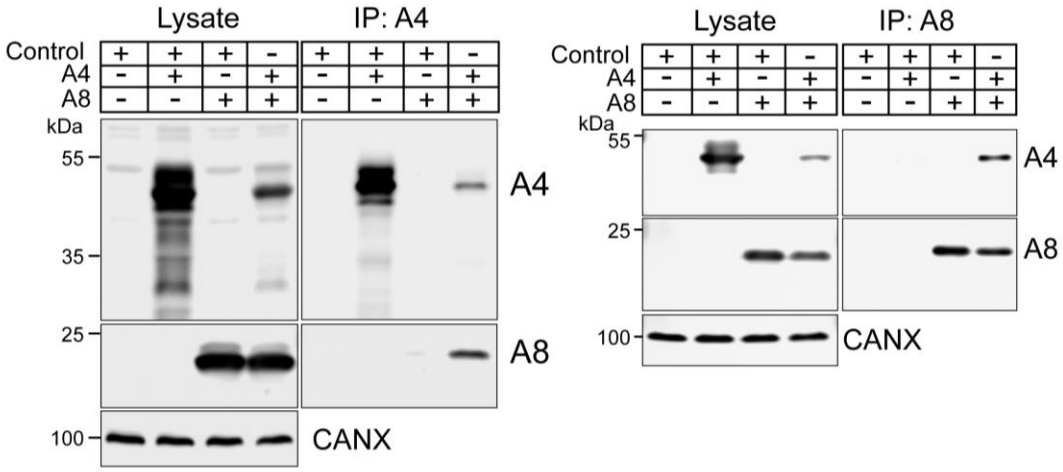

Figure S6

A8 and A4 physically interact in CHO-K1 cells. Recombinant A4-myc and A8-Flag were co-expressed in CHO-K1 cells alone (with empty plasmid) or together. A4 was immunoprecipitation using Myc-linked magnetic beads (left panel) and A8 was immunoprecipitated using Flag-magnetic beads (right panel) as described in the Methods. As A4 has non-specific binding to magnetic beads, Flag-beads were eluted by 3X Flag peptide. Immunoblot analysis using anti-A4 (top), anti-A8 (middle) and anti-calnexin (CANX) Abs was performed using 30 μg of lysate (input) as described in Methods.